63-1-6

NAVWEPS REPORT 7773
NOTS TP 2754
COPY 73

SUMMARY OF INVESTIGATIONS OF HEAT-WAVE EFFECTS ON PHOTOGRAPHIC IMAGES

compiled by

Richard B. Walton
Test Department

ABSTRACT. A comprehensive report of a year's data, taken from a special range established at NOTS for study of heat wave problems, is presented. The data include micrometeorological information as well as optical and photographic results obtained at frequent time intervals at various distances and from several camera elevations.

As a result of multiple correlation analyses of these data three experiments were conducted. Results of these experiments, which demonstrate that it is possible to modify the heat wave problem by application of various ground cover materials, are also presented.

U.S. NAVAL ORDNANCE TEST STATION

China Lake, California

October 1962

U. S. NAVAL ORDNANCE TEST STATION

AN ACTIVITY OF THE BUREAU OF NAVAL WEAPONS

C. BLENMAN, JR., CAPT., USN, Commander
WM. B. McLEAN, PH.D., Technical Director

FOREWORD

Heat waves, shimmer, and mirage all represent variations from the commonly assumed isotropy, or optical homogeneity, of the atmosphere. These phenomena introduce oscillatory errors in such parameters as apparent direction, distance, and attitude of test objects, and tend to degrade the data obtained from sightings and metric photography. Heat waves, their causes, and the possibilities of alleviating their effects on data gathering have both plagued and intrigued NOTS personnel since the inception of the Station.

This report is written to correlate and summarize the considerable amount of work and data generated at this Station on the heat-wave problem. Evidently, no final conclusions have as yet been drawn. Much of the data presented here was obtained on the so-called heat-wave test range; an example of the use of this data is found in the section on ground cover study. The heat-wave range data, although too voluminous to publish in detail in this paper, is conveniently tabulated on IBM cards for electronic data processing and is thus available for further analysis.

Since this summary is written for those having a background in the physical sciences, standard theories and general procedures are not enlarged upon. The material presented has been reviewed for technical accuracy by Carroll L. Evans, Jr.

F. M. ASHBROOK, Head
Instrument Development Division

Released under
the authority of
IVAR E. HIGHBERG, Head
Test Department

NOTS Technical Publication 2754
NAVWEPS REPORT 7773

Published by . . . . . .Test Department
Manuscript 30/MS-487
Collation. . . . . Cover, 28 leaves, abstract cards
First printing . . . . . .200 numbered copies

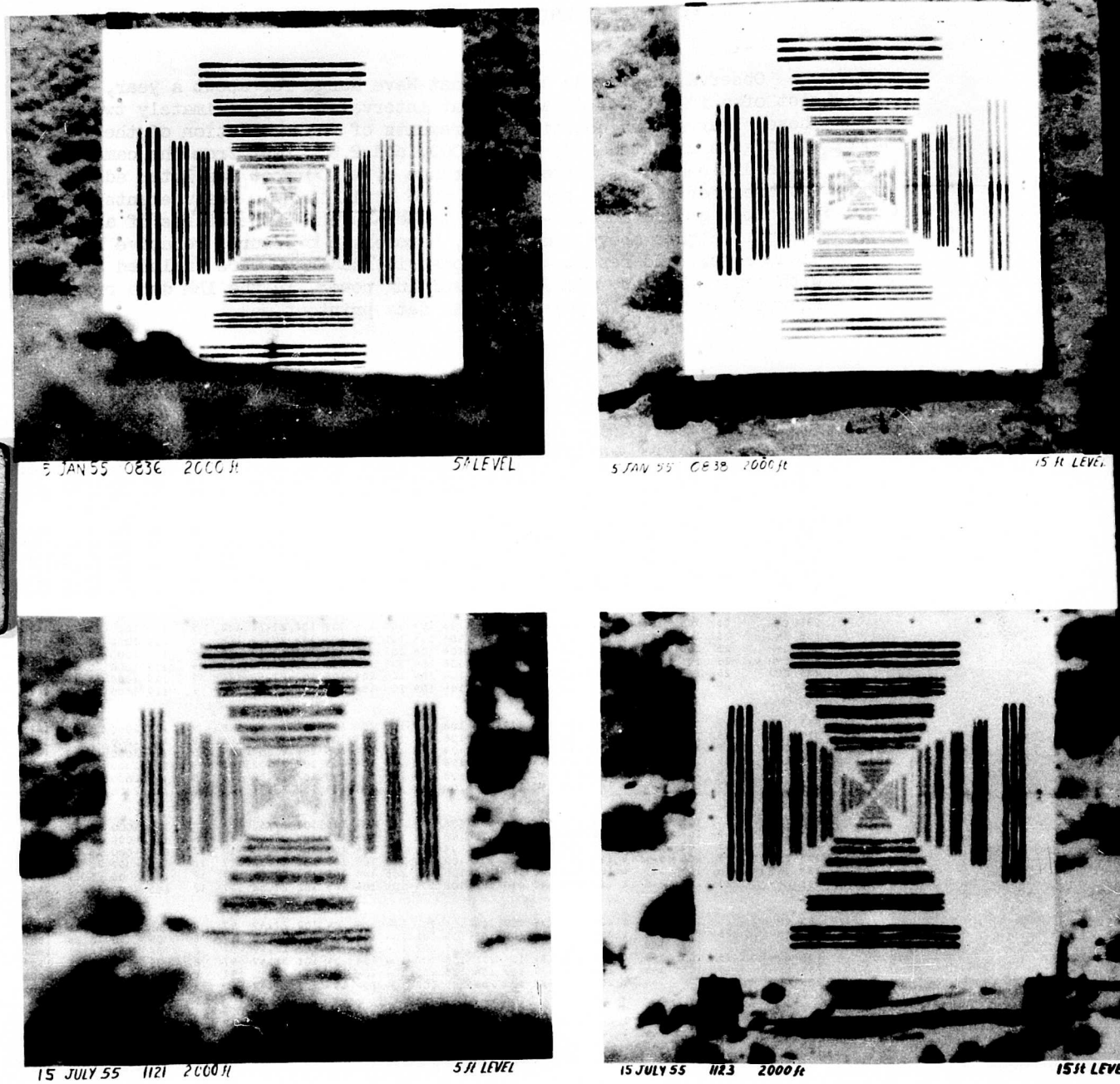

FIG. 1. Views Taken of Target Placed 2,000 ft Downrange. Note the three camer

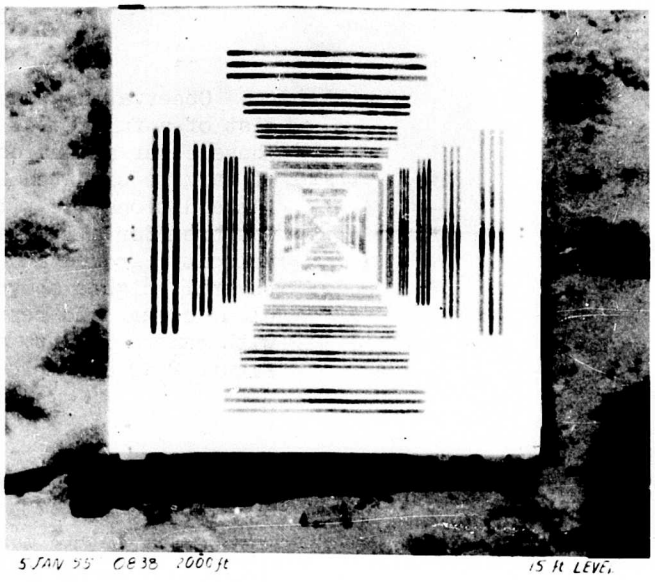

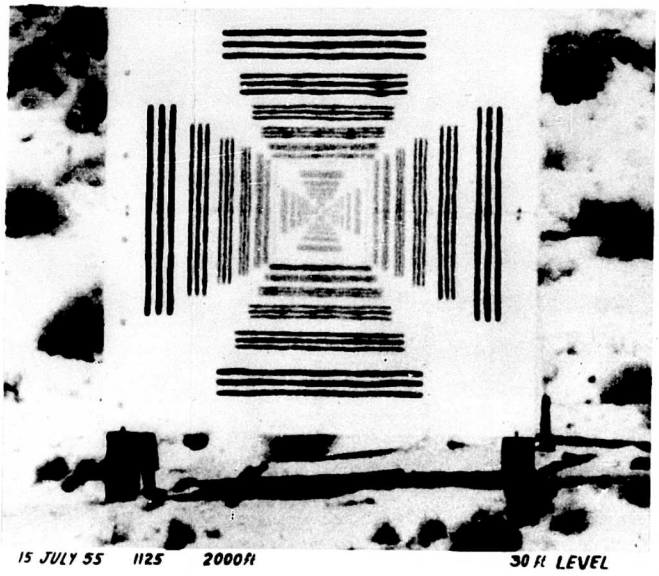

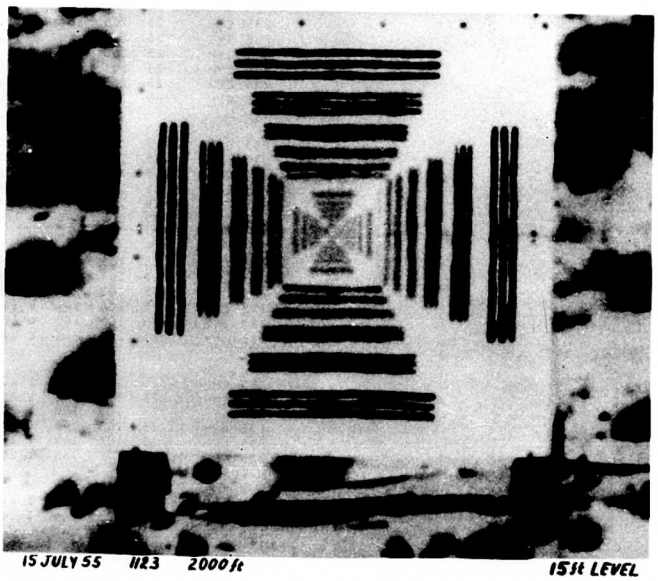

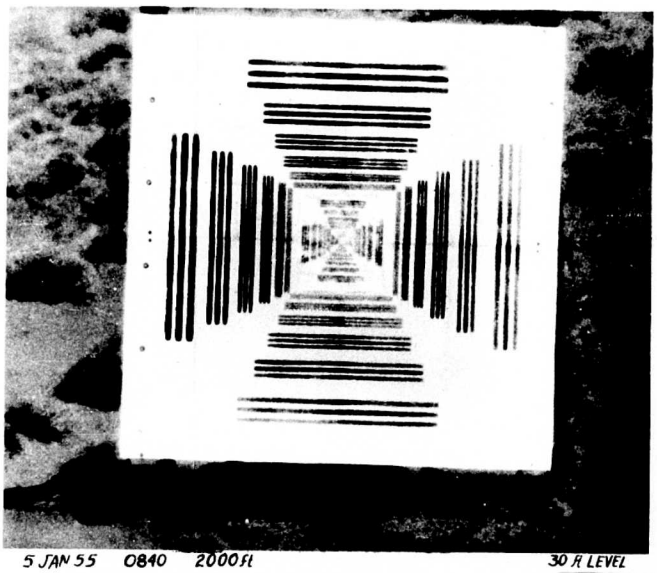

t Placed 2,000 ft Downrange. Note the three camera heights and two seasons of year shown.

2

EXPERIMENTAL RESULTS FROM HEAT-WAVE RANGE

Observations, made on the Heat-Wave Range for about a year, consist of a full day's data taken at intervals of approximately two weeks. These observations contain measurements of the resolution of the images of targets situated 250, 500, 1,000, and 2,000 feet from the camera. (An additional test target at a range of 4,000 feet was later added, and was used for all data subsequent to 8 April 1955.) Measurements of wind velocity, ground and sub-surface temperatures, temperatures of air at several heights above the ground, barometric pressure, relative humidity, cloud cover, and results of radiometric readings, were included along with camera height, time, and resolving power, in the IBM data printout. Figure 2 is a sample page from the data printout.

JULY 15

DAY	CLD CVR	VIS	TEMP	HUM	WS	WD	-.5	0	.5	2	5	10	15	25	35	45	PRES	RAD	TRANS	NCR	DIST	HT	RES	TIME
235	CMH	25	105	14%	8	160	110	140	110	108	108	104	105	104	105	102	27.52	136	12	124	250	15	20	1402
235	CMH	25	105	14%	6	160	110	140	110	108	108	104	105	104	105	102	27.52	136	12	124	250	20	19	1403
235	CMH	25	105	14%	8	160	110	140	110	108	108	104	105	104	105	102	27.52	136	12	124	250	25	19	1404
235	CMH	25	105	14%	6	160	110	140	110	108	108	104	105	104	105	102	27.52	136	12	124	250	30	19	1405
235	CMH	25	105	14%	8	160	110	140	110	108	108	104	105	104	105	102	27.52	136	12	124	500	5	8	1408
235	CMH	25	105	14%	6	160	110	140	110	108	108	104	105	104	105	102	27.52	136	12	124	500	10	14	1409
235	CMH	25	105	14%	6	160	110	140	110	108	108	104	105	104	105	102	27.52	136	12	124	500	15	16	1410
235	CMH	25	105	14%	6	160	110	140	110	108	108	104	105	104	105	102	27.52	136	12	124	500	20	14	1411
235	CMH	25	105	14%	6	160	110	140	110	108	108	104	105	104	105	102	27.52	136	12	124	500	25	16	1412
235	CMH	25	105	14%	8	160	110	140	110	108	108	104	105	104	105	102	27.52	136	12	124	500	30	16	1413
235	CMH	25	105	14%	8	160	110	140	110	108	108	104	105	104	105	102	27.52	128	9	119	1000	5	8	1415
235	CMH	25	105	14%	8	160	110	140	110	108	108	104	105	104	105	102	27.52	128	9	119	1000	10	11	1416
235	CMH	25	105	14%	8	160	110	140	110	108	108	104	105	104	105	102	27.52	128	9	119	1000	15	11	1417
235	CMH	25	105	14%	8	160	110	140	110	108	108	104	105	104	105	102	27.52	128	9	119	1000	20	11	1418
235	CMH	25	105	14%	6	160	110	140	110	108	108	104	105	104	105	102	27.52	128	9	119	1000	25	16	1419
235	CMH	25	105	14%	8	160	110	140	110	108	108	104	105	104	105	102	27.52	128	9	119	1000	30	16	1420
235	CMH	25	105	14%	8	160	110	140	110	108	108	104	105	104	105	102	27.52	128	9	119	2000	5	16	1422
235	CMH	25	105	14%	6	160	110	140	110	108	108	104	105	104	105	102	27.52	128	9	119	2000	10	8	1423
235	CMH	25	105	14%	6	160	110	140	110	108	108	104	105	104	105	102	27.52	128	9	119	2000	15	9	1424
235	CMH	25	105	14%	8	160	110	140	110	108	108	104	105	104	105	102	27.52	128	9	119	2000	20	10	1425
235	CMH	25	105	14%	8	160	110	140	110	108	108	104	105	104	105	102	27.52	128	9	119	2000	25	11	1426
235	CMH	25	105	14%	6	160	110	140	110	108	108	104	105	104	105	102	27.52	128	9	119	2000	30	14	1427
235	CMH	25	105	14%	8	160	110	140	110	108	108	104	105	104	105	102	27.52	128	9	119	4000	5	7	1428
235	CMH	25	105	14%	8	160	110	140	110	108	108	104	105	104	105	102	27.52	128	9	119	4000	10	10	1429
235	CMH	25	105	14%	8	160	110	140	110	108	108	104	105	104	105	102	27.52	117	12	105	4000	15	10	1430
235	CMH	25	105	14%	6	160	110	140	110	108	108	104	105	104	105	102	27.52	117	12	105	4000	20	11	1431
235	CMH	25	105	14%	8	160	110	140	110	108	108	104	105	104	105	102	27.52	117	12	105	4000	25	11	1432
235	CMH	25	105	14%	6	160	110	140	110	108	108	104	105	104	105	102	27.52	117	12	105	4000	30	12	1433
235	CMH	25	105	14%	1	205	112	139	109	106	105	102	104	104	104	102	27.49	97	8	89	250	5	16	1500
235	CMH	25	105	14%	1	205	112	139	109	106	105	102	104	104	104	102	27.49	97	8	89	250	10	18	1501
235	CMH	25	105	14%	1	205	112	139	109	106	105	102	104	104	104	102	27.49	97	8	89	250	15	21	1502
235	CMH	25	105	14%	1	205	112	139	109	106	105	102	104	104	104	102	27.49	97	8	89	250	20	19	1503
235	CMH	25	105	14%	1	205	112	139	109	106	105	102	104	104	104	102	27.49	97	8	89	250	25	19	1504
235	CMH	25	105	14%	1	205	112	139	109	106	105	102	104	104	104	102	27.49	97	8	89	250	30	11	1505
235	CMH	25	105	14%	1	205	112	139	109	106	105	102	104	104	104	102	27.49	97	8	89	500	5	14	1508
235	CMH	25	105	14%	1	205	112	139	109	106	105	102	104	104	104	102	27.49	97	8	89	500	10	18	1509
235	CMH	25	105	14%	1	205	112	139	109	106	105	102	104	104	104	102	27.49	97	8	89	500	15	20	1510
235	CMH	25	105	14%	1	205	112	139	109	106	105	102	104	104	104	102	27.49	97	8	89	500	20	18	1511

FIG. 2. A Typical Printout Page From Heat Wave Range Data.

PROCEDURE

Each target was photographed with the camera at heights of 5, 10, 15, 20, 25, and 30 feet above ground level, the nearer targets being photographed first. The intervals between successive exposures at various levels approximated one minute--the usual time required to raise the camera, center the field of view, and make the exposure. Occasional departures were made from the above sequence (particularly at dawn or at dusk) in order to photograph a specific target when it was best illuminated.

All exposures were made at full aperture, f/8. Accommodation for the changing illumination of the targets was achieved by varying the frame rate and shutter opening, and by use of neutral density filters. The camera's minimum exposure of 1/1152 second required the use of filters at full aperture in full midday sunlight. Unfortunately, maximum exposures of 1/250 second were used for the circumstance of weak light, since at that time this range of exposure times was supposed to have only negligible effect on the resolution. Information acquired later on in this study (see section on Peregrinations of Optical Images, and also Appendix B) suggests that the deterioration of image resolution was, in certain cases, traceable to the prolonged exposure of 1/250 second.

ASSESSMENT OF RECORDS

Each run of the camera used three or more feet of film. Ten of the fifty or more individual frames were selected randomly for assessment of image resolution. A 100-power microscope was used in reading the film. The criterion for resolution was simply whether or not the individual lines in a group could be recognized. There were four sets of lines on each resolution target, two horizontal and two vertical. Since ten frames were measured at each camera-target situation, the value for image resolution used was the mean of ten determinations. The error in the mean value for the resolution for any given time was less than one line for values of the order of 20 lines/mm. Figure 3 shows distribution of resolving power attained from photographs taken during the period November 1954 to November 1955.

THE OBSERVATIONS

Each camera target record was punched on an IBM card containing the corresponding meteorological data, camera height, target distance, time, date, and resolution. More than 6,500 such cards resulted from the year's observations. The general trend of the results is shown in Figs. 4-8. The data for these figures have been chosen as representative samples of the four seasons. The reader should note the following: (1) Resolution improves with camera height, (2) resolution is poorest in summer and in early afternoon, and (3) resolution deteriorates only slightly at increasing target distance, and even less at camera heights above fifteen feet.

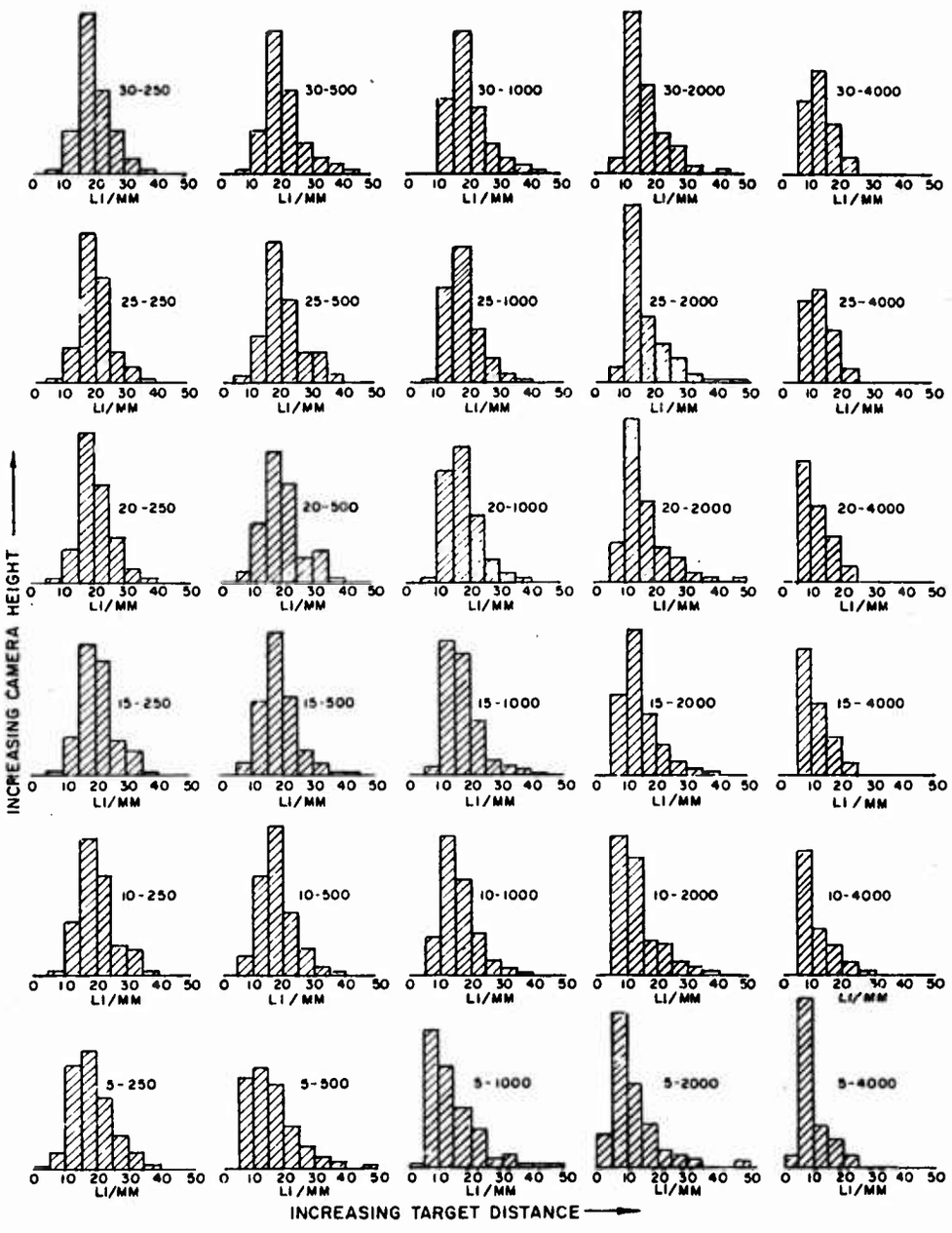

FIG. 3. Histograms Showing the Distribution of Resolving Power Obtained From Photographs Taken During the Period November 1954 to November 1955. Camera heights of 5, 10, 15, 20, 25, and 30 feet were used to photograph targets at distances of 250, 500, 1,000, 2,000, and 4,000 feet. The height-distance combination is included next to each histogram.

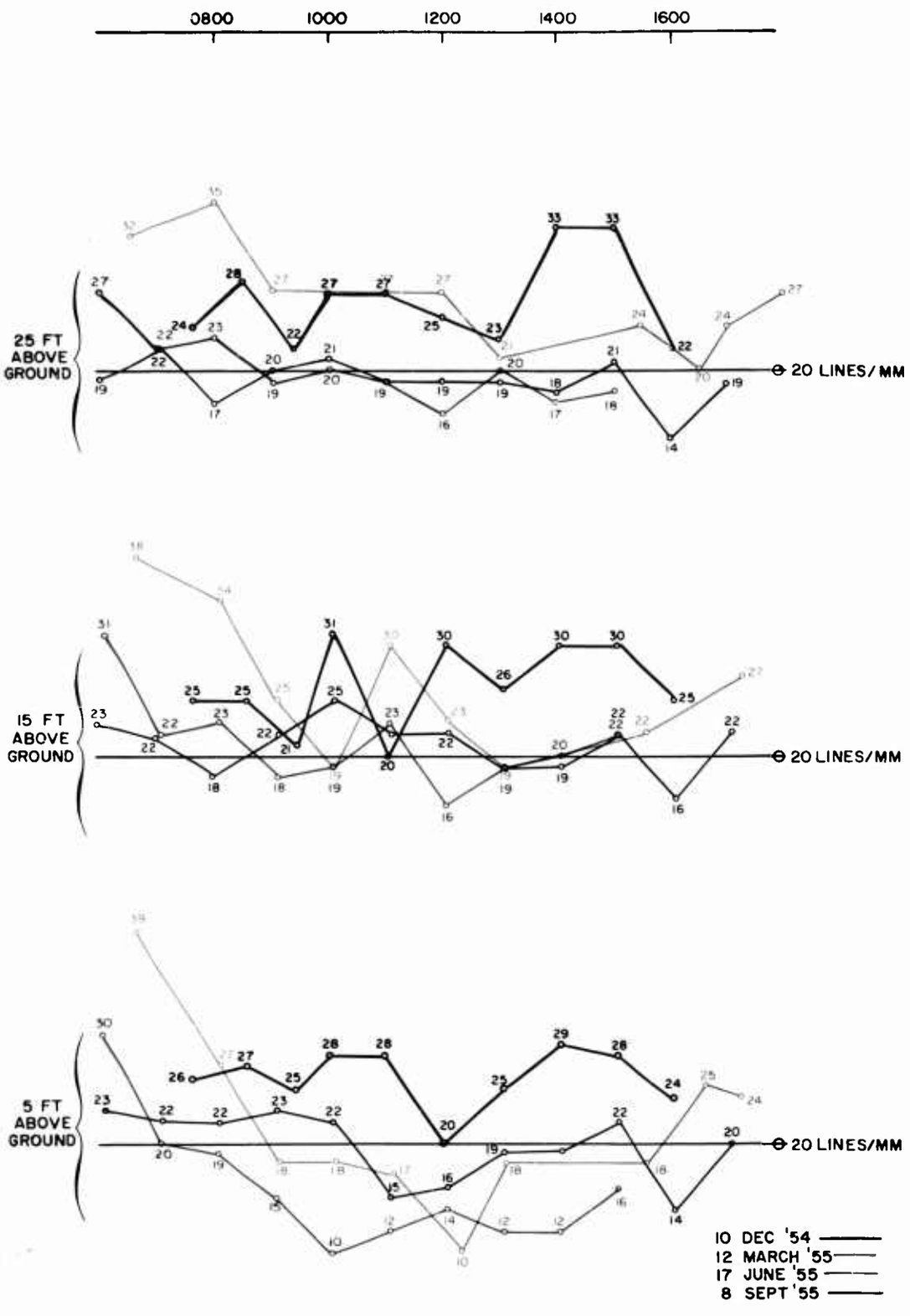

FIG. 4. Diurnal Variation of Atmospheric Effects on Image Resolution Plotted From Data Recorded at Three Camera Heights on a Specific Day From Each Season. Target was positioned 250 ft downrange.

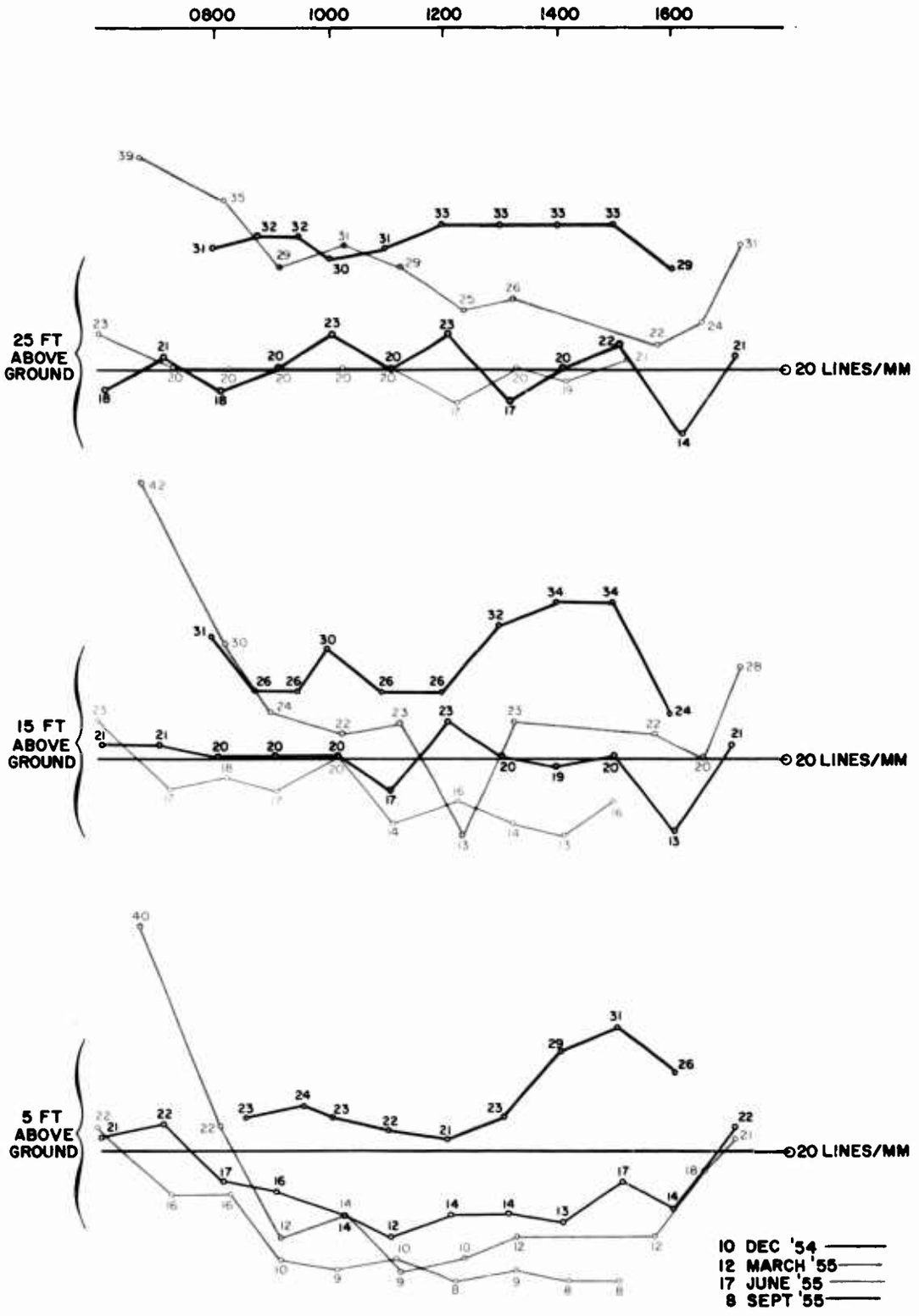

FIG. 5. Diurnal Variation of Atmospheric Effects on Image Resolution Plotted From Data Recorded at Three Camera Heights on a Specific Day From Each Season. Target was positioned 500 ft downrange.

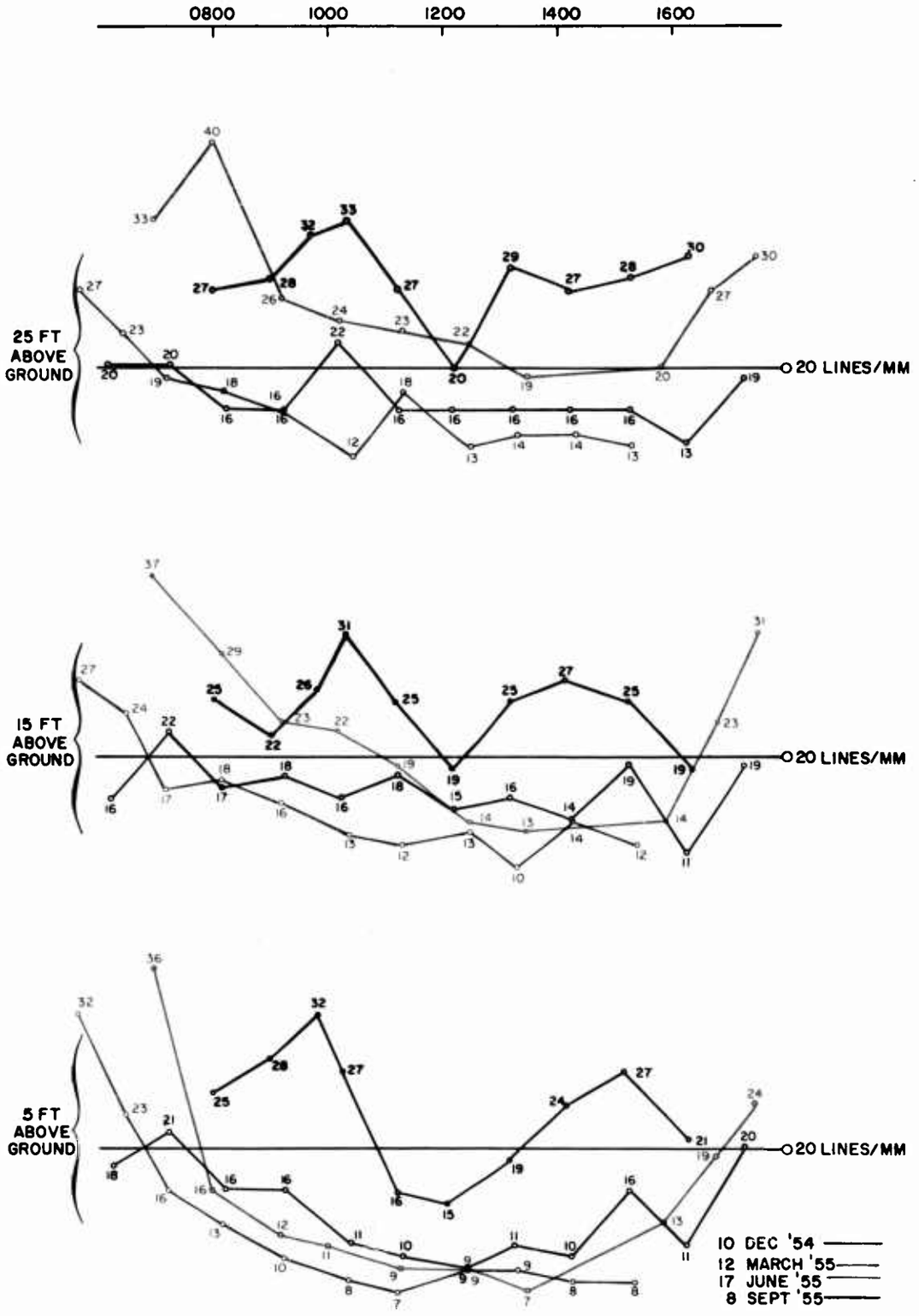

FIG. 6. Diurnal Variation of Atmospheric Effects on Image Resolution Plotted From Data Recorded at Three Camera Heights on a Specific Day From Each Season. Target was positioned 1,000 ft downrange.

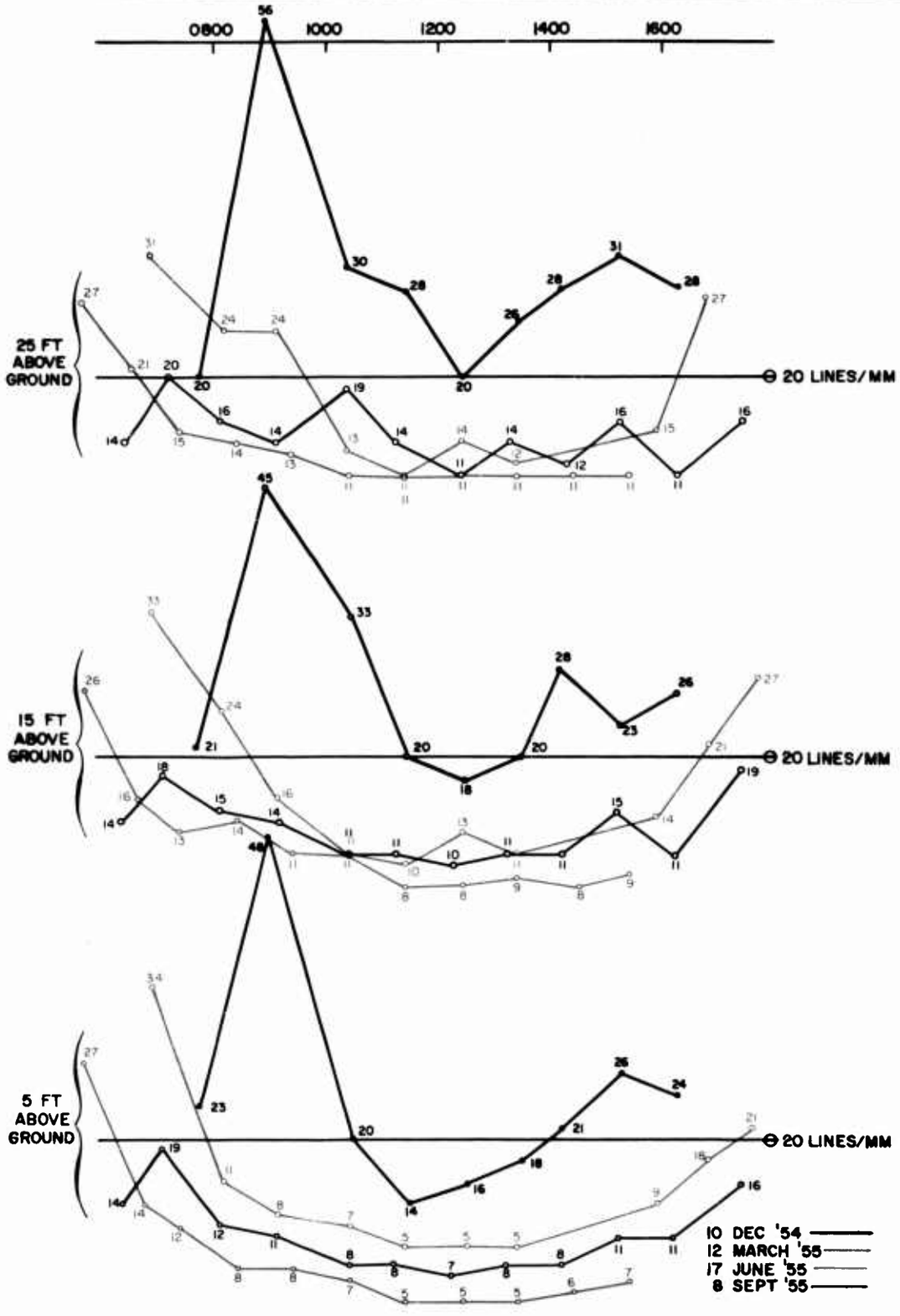

FIG. 7. Diurnal Variation of Atmospheric Effects on Image Resolution Plotted From Data Recorded at Three Camera Heights on a Specific Day From Each Season. Target was positioned 2,000 ft downrange.

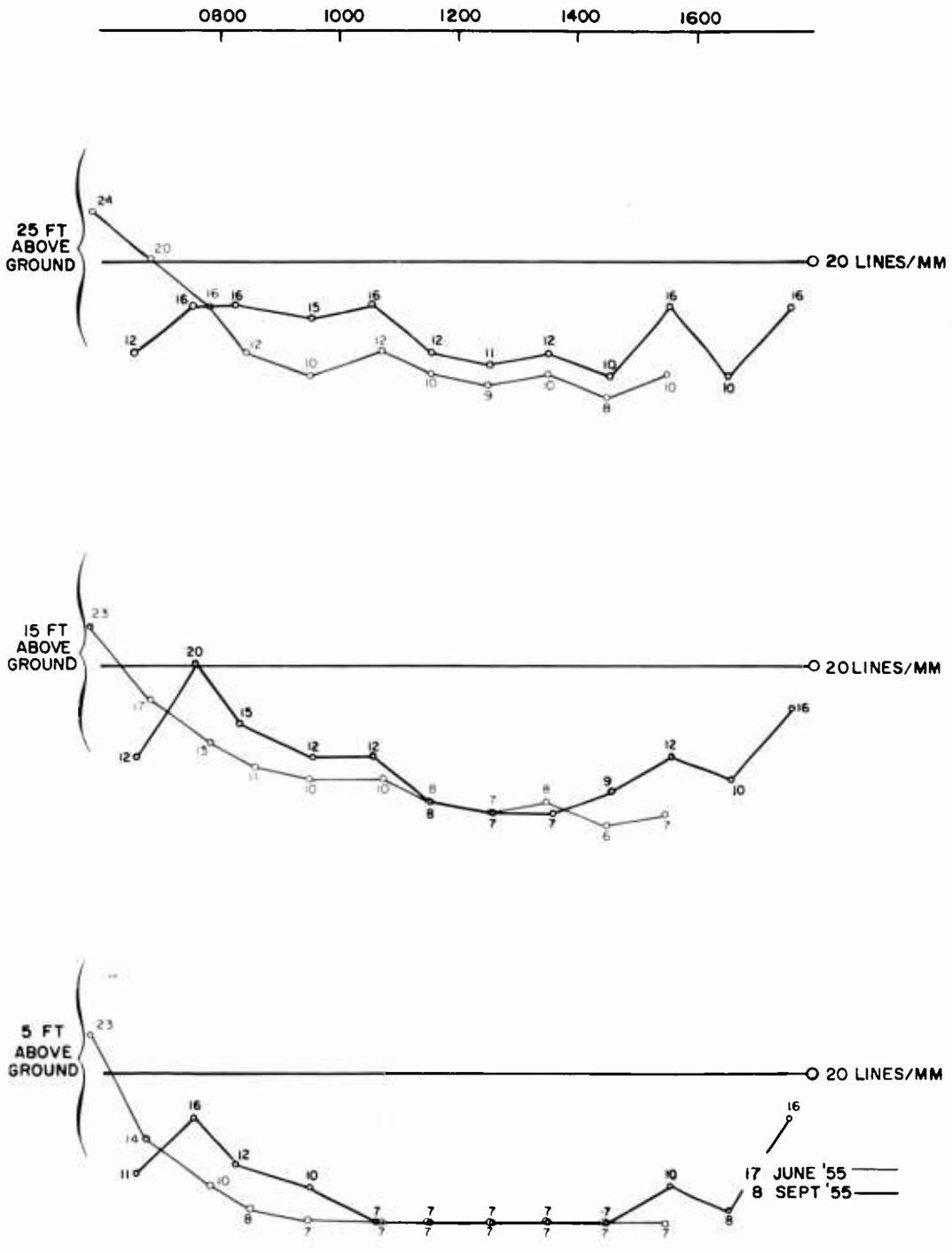

FIG. 8. Diurnal Variation of Atmospheric Effects on Image Resolution Plotted From Data Recorded at Three Camera Heights on a Specific Day From Summer and Autumn. Target was positioned 4,000 ft downrange.

PEREGRINATIONS OF OPTICAL IMAGES

The faithful depiction of distant objects over a desert terrain is degraded by the presence of intervening moving masses of air which, because they are at different temperatures, have different densities and hence different indices of refraction. These parcels of moving air may assume various shapes and sizes. The motion and expected lens-like behavior of these parcels continually produce a wide scope of variations in the directions and lengths of optical paths, thus giving rise to the phenomena of mirage, looming, and heat waves. The image of a distant object is therefore seen, under moderate magnification, to be altered in either or both of the following ways:

Distorted. The subdivisions of the image are shifted more or less in random fashion as to direction and time of shift, or are thrown out of focus, so that the image is blurred perhaps beyond recognition.

Displaced. The image as a whole is transported rapidly in a more-or-less random fashion as to direction and time of shift, about a mean position, so that the image, though oscillating wildly, is fairly well defined and essentially undistorted.

The moving masses of air of varying physical and optical density are called "turbulons" by Becker (Ref. 1). He defines a single turbulon as a volume of gas or fluid having an index of refraction differing significantly from that of the surrounding gas. It is desirable to further classify the turbulons in regard to size. For this study, a "small" turbulon refers to a parcel or module of optically inhomogeneous air which subtends a small angle from the viewpoint of the camera; small turbulons give rise to the first alteration of the image listed above, i.e., distortion. A "large" turbulon is simply one that subtends a large angle at the camera and hence gives rise to the second alteration of image cited above, i.e., displacement.

One approach to an analysis of the heat-wave problems depends upon a model of the lower atmosphere involving both descending cold masses of denser air and rising masses of less-dense warm air (Ref. 6)*. The descending turbulons might be expected to act much like cylindrical positive lenses, whereas the rising turbulons might be expected to behave as cylindrical negative lenses. Wood (Ref. 34, p. 89) has discussed experimental work with lenses of gelatin soaked in various materials such as glycerine, which exhibit similar behavior. Certain aspects of this lens behavior are expected to differ from those of the usual glass lens,

*In Ref. 6 Cone describes an interesting vortex model of rising warm air mass arising from mushroom shaped warm air modules present near ground.

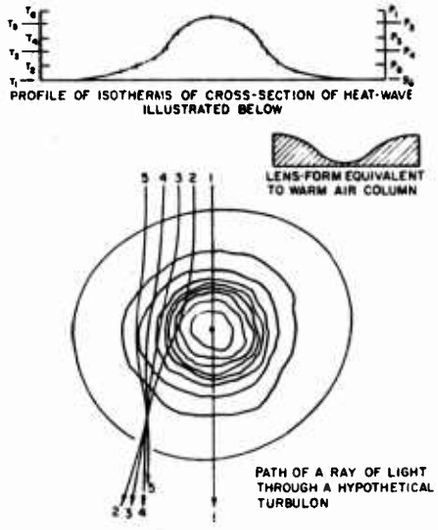

FIG. 9. Three Aspects of Turbulon Resulting From Rising Warm Air.

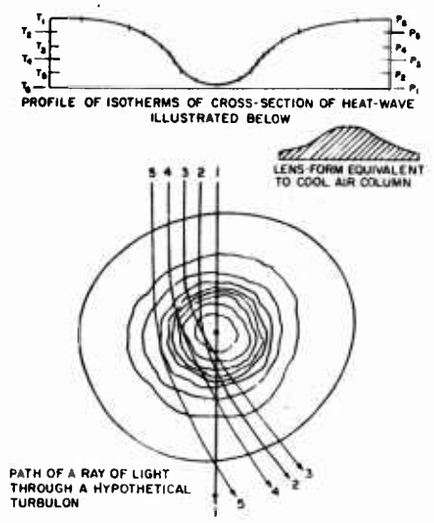

FIG. 10. Three Aspects of Turbulon Resulting From Cool Descending Air.

chiefly in that (1) the index of refraction will not be uniform within the turbulon, but will vary with only a small difference from surrounding air at surface and a larger difference nearer the center, (2) the turbulons will not be, in general, perfectly cylindrical, but rather distorted, (3) the turbulons will not be stationary but will vary with time, perhaps with temporary large changes occurring, from time to time, in the diameter of a turbulon with spheroidal modules rising or falling, where before there was but a small-diameter cylinder. Figures 9 and 10 illustrate this concept of the deviation of parallel light paths by such simple cylindrical hot and cold air masses.

An Experimental study has been undertaken in which a motion picture record made over a 500-foot path essentially parallel to and five feet above a typical desert terrain was analyzed. A study of the amount and pattern of relative motion of portions of the image is described with some mathematical detail in Appendix B. The record is in two parts, one made under good and the other made under poor seeing conditions.

GROUND COVER STUDIES

Small-scale tests were performed by Evans and Lyon to determine the effect, if any, of various ground covers on some of the factors affecting photographic resolution. The ground covers investigated were lime, grass, and simple water sprinkling. In each test a typical untreated desert area was used for control purposes.

Of the total solar energy incident upon the surface of the earth, Et, a portion is reflected from the surface and a portion is absorbed by the ground. The energy radiated from the ground combined with that reflected, is called E_r. The energy conducted into the soil is called Eg. Net convective remainder, NCR, is considered to be the incident solar energy less the portions reflected and absorbed. Thus,

$$NCR = E_t - E_r - E_g.$$

Stewart and MacCready (Ref. 10) have used a similar concept and referred to it as,"... the convective heat transfer through the air."

A 10% sample of the IBM cards selected at random from the year long series of observations was subjected to multiple regression analysis. The resulting relationship between resolution, NCR, target distance, camera height, and temperature is presented in Appendix C along with other experimental details of ground cover tests. Figure 11 shows the relationships of NCR, resolving power, and temperature. A marked improvement in the theoretical resolution was found for the limed area.

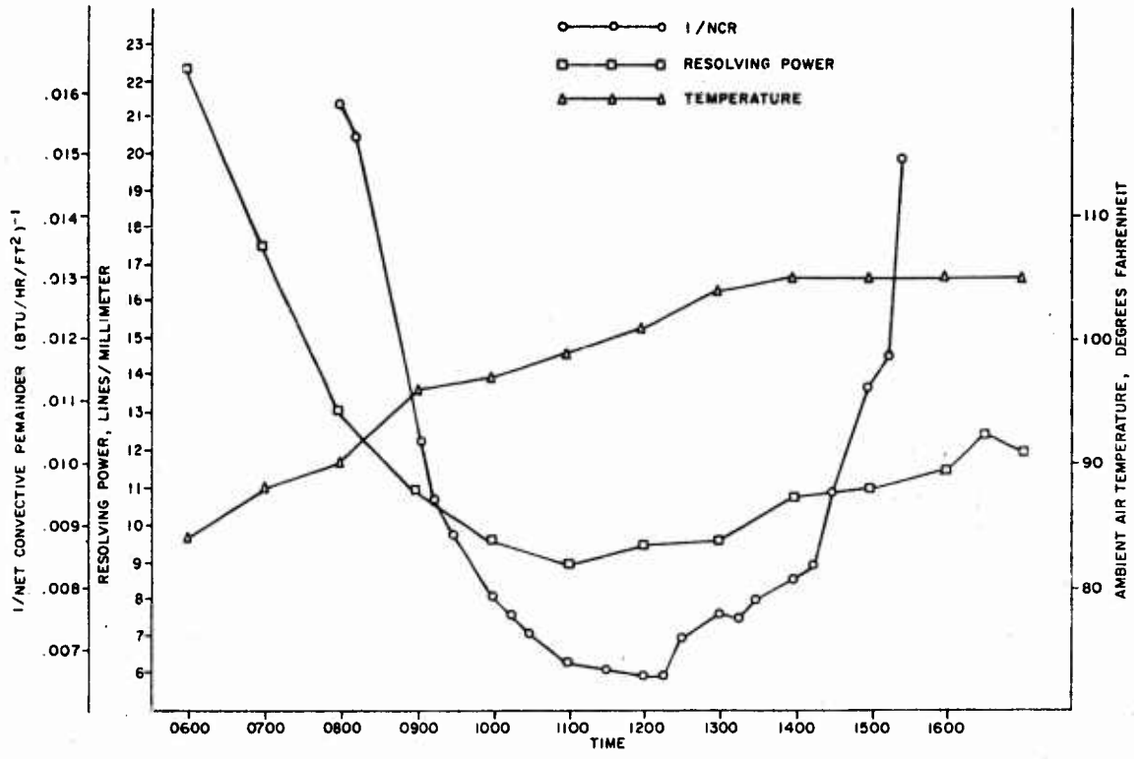

FIG. 11. Average Resolving Power, Ambient Air Temperature, and the Reciprocal of Net Convective Remainder Are Shown as Functions of Time. Resolving power targets were photographed from a distance of 2,000 feet over desert terrain, on July 15, 1955.

CONCLUSIONS AND RECOMMENDATIONS

Several aspects of the heat wave problem have been investigated. Results of experiments on a special heat wave range for a period of over a year have been analyzed. Three experiments in ground cover modification have demonstrated the relevance of the turbulon model.

The conditions which give rise to heat waves are temperature inversion, clear skies, and absence of winds--in other words, atmospheric instability. The effects of heat waves on photographic data can be alleviated in part by use of elevated camera positions and by modification of ground cover.

The net convective remainder is a useful concept in predicting the resolution of photographic images from meteorological data. Figure 12 shows a significant, but not singular, dependence of resolution upon NCR.

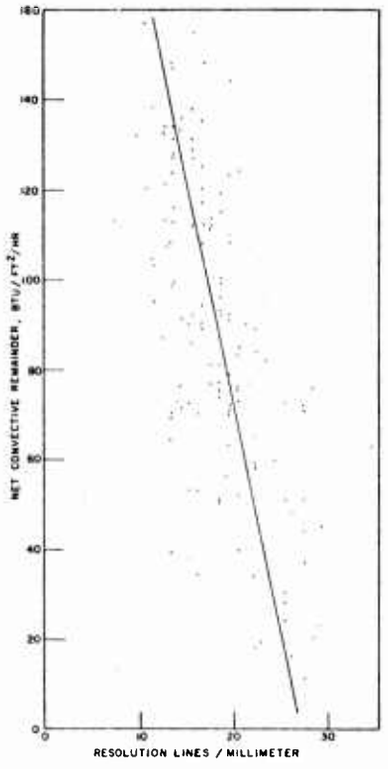

FIG. 12. Plot of Resolution Vs NCR.

Ambient temperature, wind velocity, time of day, and time of year are other factors which seem important in predicting resolution. An attempt at a further multiple regression analysis of these factors and NCR might constitute a reasonable problem for future investigation.

The pattern of diurnal variation, with optimum conditions existing during early morning and late afternoon hours, is modified in degree by seasonal variation, with optimum conditions occurring from Fall to early Spring. The pertinent data seem to indicate the following as prudent courses of action: (1) insofar as possible, conduct tests at night so as to utilize the quiescent atmosphere, (2) establish criteria for anticipated resolution minima based on NCR, and (3) cancel photographic coverage of tests for which a useless photographic record is indicated.

The results of these studies have shown our atmosphere to be so imperfect a medium that daytime use of photographic instruments having least counts appreciably smaller than five seconds of arc may represent useless extravagance.

Appendix A

HEAT-WAVE RANGE INSTRUMENTATION

The heat wave range is located on the eastern side of the Indian Wells Valley and extends 4,000 feet northwestward from the base of the K-2 launcher, as shown in Fig. 13. Northeast and east of the heat wave range is the Argus range of mountains with elevations above 6,000 feet m.s.l., and to the west and southwest is a dry lakebed with an elevation of 2,200 feet m.s.l. The heat wave range runs nearly parallel to the contour lines along the lowest foothills of the Argus mountains at an estimated elevation of 2,300 feet m.s.l. Sandy soil and semidesert vegetation predominate over the entire test range area.

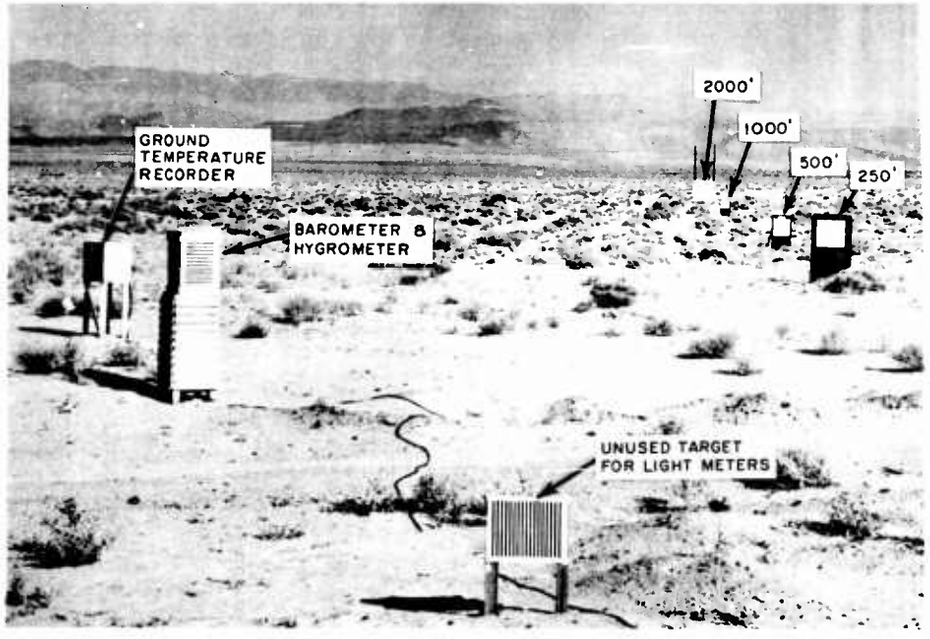

FIG. 13. Heat Wave Range Viewed From Camera Position. Test targets are shown at 250, 500, 1,000, and 2,000 feet downrange; the target at 4,000 feet was added later.

The following variables are measured: wind direction and speed at heights of 4 feet and 20 feet, ambient air temperature at eight heights, ground temperature at two levels below the surface, relative humidity, atmospheric pressure, net solar and terrestrial radiant exchange, and the heat flux conducted into the ground.

Visibility is estimated in accordance with the U. S. Weather Bureau standards and known visibility markers.

Sky cover and the height and type of clouds are also estimated according to Weather Bureau standards and, whenever possible, cloud heights are checked from pilot observations over the ranges and by means of ceiling balloons used by the Aerology Office at Armitage Field. This field is approximately eight miles southwest of the heat wave range, as shown in Fig. 14.

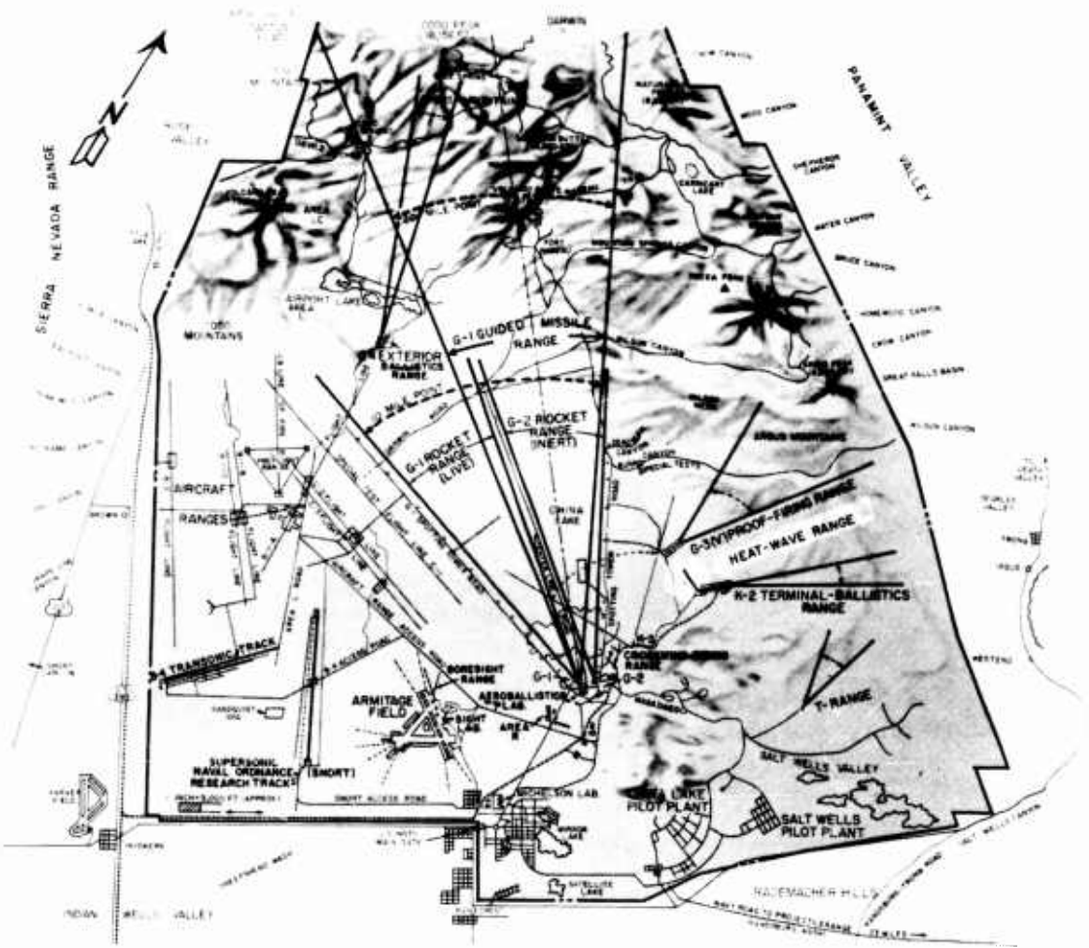

FIG. 14. Location of the Heat Wave Range with Respect to Other NOTS Ranges and Access Roads.

Pyrheliometer, winds aloft, and radiosonde data are collected for test days. Records are also kept of air mass conditions and the general synoptic situation both at the surface and aloft.

Listed below are the major types of data gathered and the instruments used:

1. Wind direction and speed: two Beckman Whitley wind speed and direction recorders.

2. Humidity: Bendix-Friez hygrothermograph and a motor psychrometer are used to measure humidity.

3. Air Temperature: ambient air temperature is measured by a mercurial thermometer in a thermoscreen, and is also measured at eight heights on a telephone pole (Fig. 15).

4. Atmospheric pressure: pressure measurements are recorded by a Bendix-Friez microbarograph.

5. Ground temperature: a micromax recorder and two thermohms sense and record the ground temperature at two levels below the earth's surface.

6. Net radiant exchange: the net radiant exchange is measured by Beckman-Whitley radiometers and recorded by a Brown Electronik Strip Chart Recorder.

7. Ground conduction: heat energy conducted into the ground is measured by Beckman-Whitley Heat Flow Transducers and recorded by a Brown Electronik recorder.

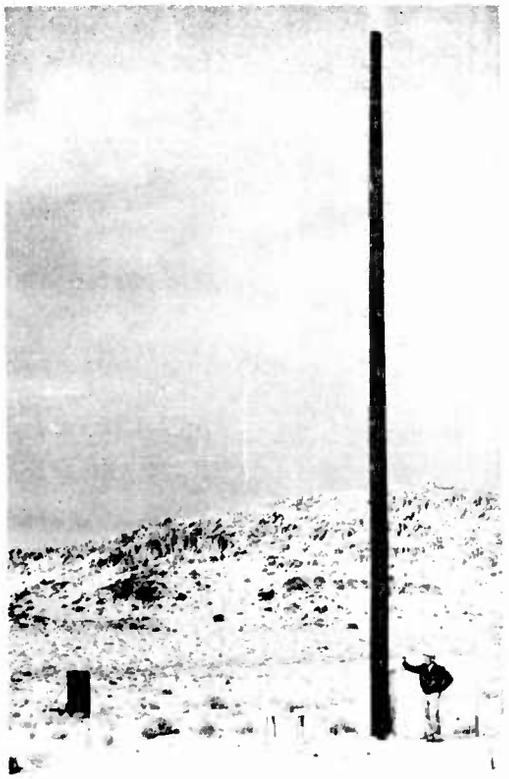

FIG. 15. Eight Thermocouples Mounted on a 45-ft Telephone Pole. Three 4x8-ft target boards used to mount resolution charts are shown at lower left

FIG. 16. Beckman & Whitley Wind Speed and Direction Recorder. The wind speed and direction sensing elements are shown in the left foreground, two Esterline Angus recorders in the right foreground, and the power supply unit in the center.

WIND DIRECTION AND SPEED

No correlation between photographic displacement of an image and the direction and speed of the wind has been found in the literature. The heat wave range, shown in Fig. 13 has been equipped with two Beckman and Whitley wind speed and direction recorders with the object of determining the effect of these two variables on the photographic images.

One recorder is placed 50 feet downrange from the camera; its sensing elements are 20 feet above the ground. The other airvane is 750 feet downrange; its sensing elements are four feet above the terrain. Figure 16 shows one of the Beckman and Whitley wind speed and direction recorders.

The Beckman and Whitley recorders have a threshold below one mph, which has been attained through the use of a very low-mass wind vane, a three-cup anemometer, and drag-free electronic transducers. The anemometer mechanism interrupts a light beam as it rotates, and this signal

is transmitted to the recorder. The manufacturer claims an average upward transient response time of approximately 1.25 seconds for the anemometer, while downward response time averages 2.25 seconds. Response of the wind vane to a 45-degree shift at three mph (or more) wind speed is 1.25 seconds. Response time increases below 3 mph. These instruments also incorporate a pen keep-alive circuit, which reduces pen-to-paper friction and causes the pen to respond more faithfully to the applied signal.

The accuracy of the manufacturer's statements concerning response times has not been checked because we are interested mostly in average wind speed and direction measurements taken over an interval of several seconds. Further investigation into the heat wave problem may indicate the need for more accurate wind speed and direction measurements.

HUMIDITY

A thermoscreen, four feet above the ground, located slightly west of the line of sight between the camera and the resolution charts, houses several thermometers, a Bendix-Friez hygrothermograph provides a continuous record of temperature (to 1°F) and humidity (to within 5%). It was decided that a more accurate method for determining the relative humidity was needed, hence a motor psychrometer was installed in the thermoscreen. With an accuracy of 1-1/2 % readings are taken hourly with this instrument on test days.

AIR TEMPERATURE

AMBIENT AIR TEMPERATURE

Ambient air temperature measurements are made continuously by the Bendix-Friez hygrothermograph, as previously mentioned, and hourly measurements are taken from a calibrated mercurial thermometer in the thermoscreen. All mercurial thermometers used in measuring temperatures for the heat-wave studies were calibrated by the NOTS Standards Laboratory, and are accurate to 0.2 deg.

TEMPERATURE GRADIENT

The determination of temperature at eight levels above the ground is accomplished by the use of miniature thermocouples placed at various heights on a telephone pole. The thermocouples are extended horizontally three feet from the pole by aluminum tubing and are located at the following heights: 0.5, 2.0, 5.0, 10.0, 15.0, 25.0, 35.0, and 45.0 feet above the ground, as shown in Fig. 15.

The thermocouples were made of No. 30 matched Leeds and Northrup copper-constantan wire. Each thermocouple bead (approximately .032 inches in diameter) was coated with basic lead carbonate and dipped in paraffin.

For calibration the thermocouples were immersed in an ice bath and the temperature readings recorded by a Brown Electronik recorder. These checks proved the thermocouples in the installation to be accurate within 0.1 deg. To check the accuracy of the thermocouples for measurements of ambient air temperature while exposed to the sun's radiation, comparisons were made in the field using a 24-inch calibrated mercurial thermometer (shaded) at three thermocouple levels. The results of these comparisons are shown in Fig. 17.

ATMOSPHERIC PRESSURE

Atmospheric pressure, important in air density calculations, is recorded by a Bendix-Friez microbarograph. This is a portable instrument with an aneroid pressure-sensing mechanism, and a specified accuracy of 0.02 inches of mercury.

Frequent checks are made on test days with the pressure readings obtained at Armitage Field (Fig. 14), where a mercurial barometer is used. Correction is made for the difference in elevation (68 feet) between K-2 range and Armitage Field.

GROUND TEMPERATURE

Subsoil temperature measurements are made with two Leeds and Northrup thermohms and a recorder. The thermohms, placed at depths of 1/2 inch and 6 inches in the natural sandy soil of K-2 range, are protected by brass covers. The protective covers increase the thermal lag, but the protection is considered necessary.

The Micromax recorder accurately records the ground temperature in degrees centigrade. This is later converted to degrees Fahrenheit for ease of comparison with ambient air temperatures near the ground. One channel of this recorder is a zero reference and serves as a convenient check for instrument drift. Expected accuracy is 1.0°F.

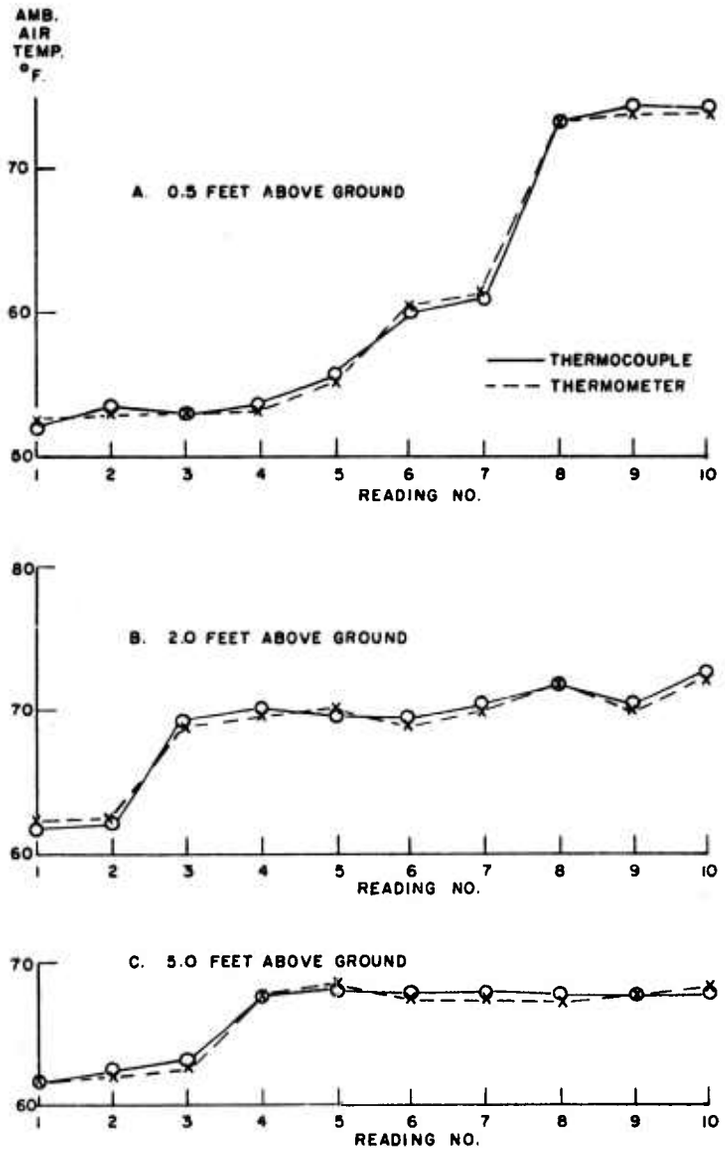

FIG. 17. Temperature Readings From Three Coated Thermocouples Positioned at 0.5, 2.0, and 5.0 Ft Elevation Compared With Readings From a Shaded Mercurial Thermometer Placed at the Same Elevations.

NET RADIANT EXCHANGE

Before describing the net exchange radiometers and the soil heat-flow transducers, which are discussed in item (7), it is useful to consider the source of the energy available for the formation of heat waves and the measurements which are necessary before a satisfactory heat wave theory can be generated.

The total amount of energy coming to the earth from the sun (E_t) is usually measured by a pyrheliometer. However, in studying heat waves we are interested only in that heat which produces density variations in the atmosphere. Therefore, we must subtract from (E_t) the energy which is re-radiated from the earth (E_r) and also the energy which is conducted down into the soil (E_g). The remainder (NCR) is theoretically the heat left for convection and the consequent formation of heat waves. In equation form this relationship may be written as

$$NCR = (E_t - E_r) - E_g.$$

A measure of the net radiant exchange ($E_t - E_r$) is obtained from Beckman-Whitley radiometers. These instruments consist primarily of thermopile transducers attached directly in front of small air blowers which eliminate undesirable convection effects. Output of the thermopile transducers is adequate for the direct driving of a Brown Electronik 12-channel recorder. Twelve seconds after sudden exposure these instruments reach 95% of steady state condition.

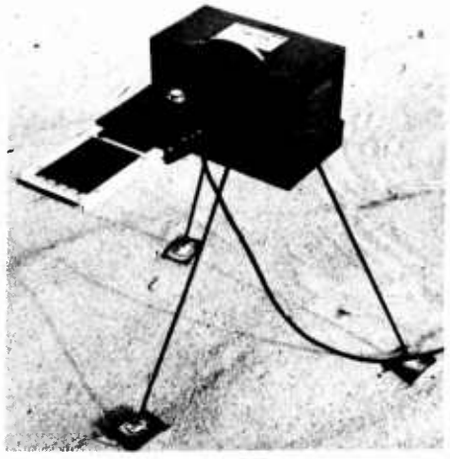

FIG. 18. Net Exchange Radiometer. The sensitive two-surface area is approximately four and a half inches square.

The net exchange radiometer shown in Fig. 18 is constructed so that the reading obtained is actually the difference between the incoming solar radiation and outgoing or reflected earth radiation; thus, it gives a measure of the energy transfer to the earth, part of which is available for the formation of heat waves.

A comparison check of two radiometers to be used in the project was made on 19 November 1954. The radiometers were placed close together over similar sand and the measurements which were made are shown in graphical form in Fig. 19.

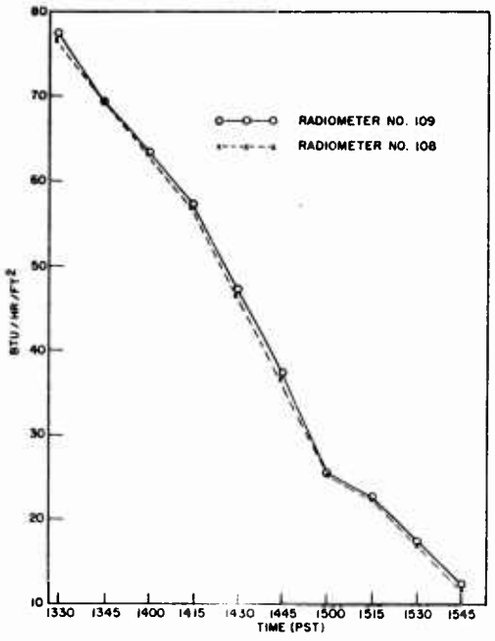

FIG. 19. Comparison of Readings Taken by Two Beckman and Whitley Net Exchange Radiometers. Instruments placed side by side over similar sand at K-2 heat wave range.

GROUND CONDUCTION

In order to measure the amount of heat available for convection, consideration must be given to the amount of heat conducted into the ground (E_g). Measurement of this energy is accomplished by a small thermopile which is buried 1/4 inch under the sand in the vicinity of the radiometers.

In operation, the thermopile produces an EMF proportional to the temperature gradient induced by heat flow through the thermal current-resisting material in the center of the transducer. A Brown Electronik Recorder is used to record this voltage. The response time for these sensing elements is 95% steady state in 12 seconds, and the accuracy of calibration is 2%.

On 23 November 1952, the two heat-flow transducers were placed side by side under 1/4 inch of sand and exposed to the direct rays of the sun. The measurements which were obtained are plotted in Fig. 20.

Figure 21 illustrates graphically how the data from a radiometer (E_t - E_r), along with the data from a heat flow transducer, are used to determine the net convective remainder, NCR.

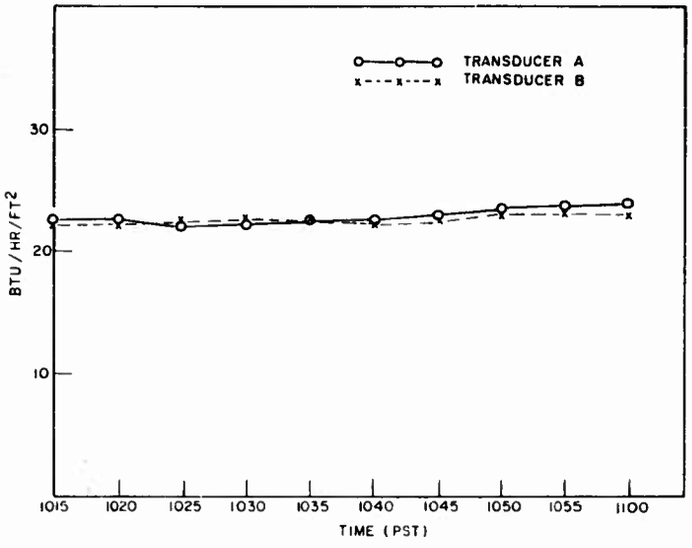

FIG. 20. Comparison of Readings Taken by Two Beckman and Whitley Soil Heat Flow Transducers. These instruments were buried side by side under 1/4 in. of sand at the K-2 heatwave range.

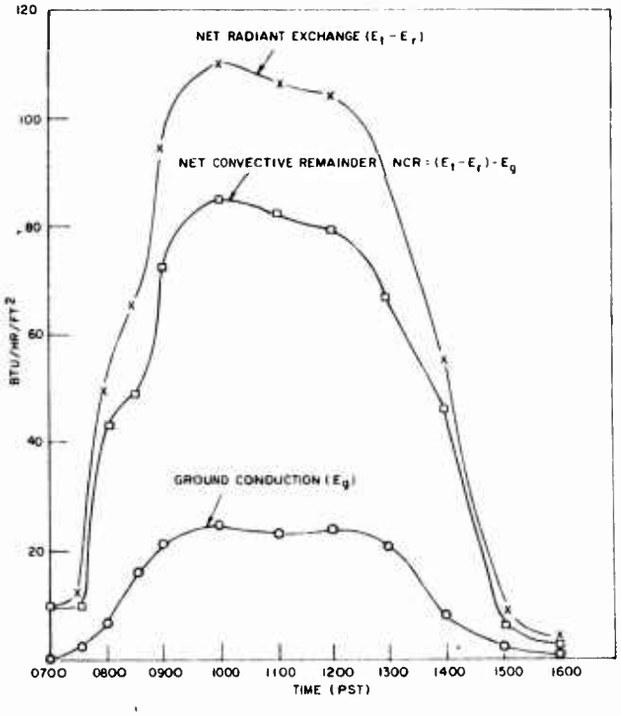

FIG. 21. Graph Showing How the Measurements of (E_t - Er) From a Radiometer, and Measurements of E_g From a Soil Heat Flow Transducer Are Used to Determine the Net Convective Remainder (NCR).

Appendix B*

PEREGRINATIONS OF OPTICAL IMAGES

It was the object of this study to determine the character, location, and effect of turbulons on the quality of photographic images, and to develop a method of data reduction that would separate the image motion caused by turbulons from the image motion caused by other factors, such as camera vibration.

METHOD OF DATA ACQUISITION

Data for this study were acquired by photographing the target shown in Fig. 22 across 500 feet of typical desert terrain. The items of chief interest were the four small disks in a three-foot square array, which was attached to the corners of an enlarged reproduction of the 1952 resolution chart of the National Bureau of Standards. A Mitchell 35/mm motion-picture camera equipped with a Thompson lens having a focal length of 48 inches and an aperture ratio of f/8 was used. The camera was loaded with Linagraph-Ortho film and operated at 16 frames per second with a 10 deg. shutter opening. The line-of-sight was five feet above ground level.

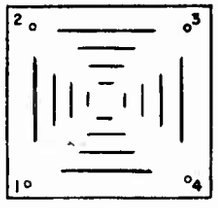

FIG. 22. Chart Used as the Photographic Object.

Two sets of data were acquired and are tabulated below. One set was gathered early in the morning, the other early in the afternoon in order to obtain one set when the temperature gradient near the ground was small and another when the gradient was large.

---

*The material presented in Appendix B has been abstracted from an unpublished manuscript entitled "On the Peregrinations of Optical Images of an Object Caused by Heat Waves" written by the late W. H. Christie and partially revised by H. F. Pearl.

Observational Data

No.	Time PST 4/29/54	Sky	Wind		Temp.		Seeing*	Remarks
			Vel (mph)	Dir (°Az)	Ground temp (°F)	Air temp (°F)		
1	0715	scat. clouds	1-3	270	73	60	6	visibility: 30 miles
8	1400	cir. & cum.	15	260	118	77	1-2	cloud shadows over target

*Seeing is a subjective term used by astronomers in an attempt to estimate the steadiness or clarity of an image. It is rated on a scale of 1 to 10, where 1 is very poor and 10 is perfect. 6 is considered good, corresponding to the resolution of 18 lines/mm on a photograph of the resolution chart in this study.

METHOD OF DATA REDUCTION

The exposed film was inserted into the Borereader film-measuring machine and the locations of the centers of Disks 1, 2, 3, and 4 determined for each frame in the X and Y directions. The X and Y coordinates were subscripted 1, 2, 3, and 4 for the respective points, and were referred to the sprocket holes in the film. The results are plotted in Fig. 23. In general, the X and Y values of each disk varied from frame to frame on account of the apparent displacement of the disk due to the following factors as produced under conditions of this experiment:

1. Camera movement (vibration and flexure of the tripod mount).
2. Image distortion by a small turbulon.
3. Image shift by a large turbulon.

The numerical subscripts are subscripted c, h, and H to indicate these three factors, respectively. The centers of Disks 1, 2, 3, and 4 are called Points 1, 2, 3, and 4 respectively, and their coordinates are called the coordinates of the disks.

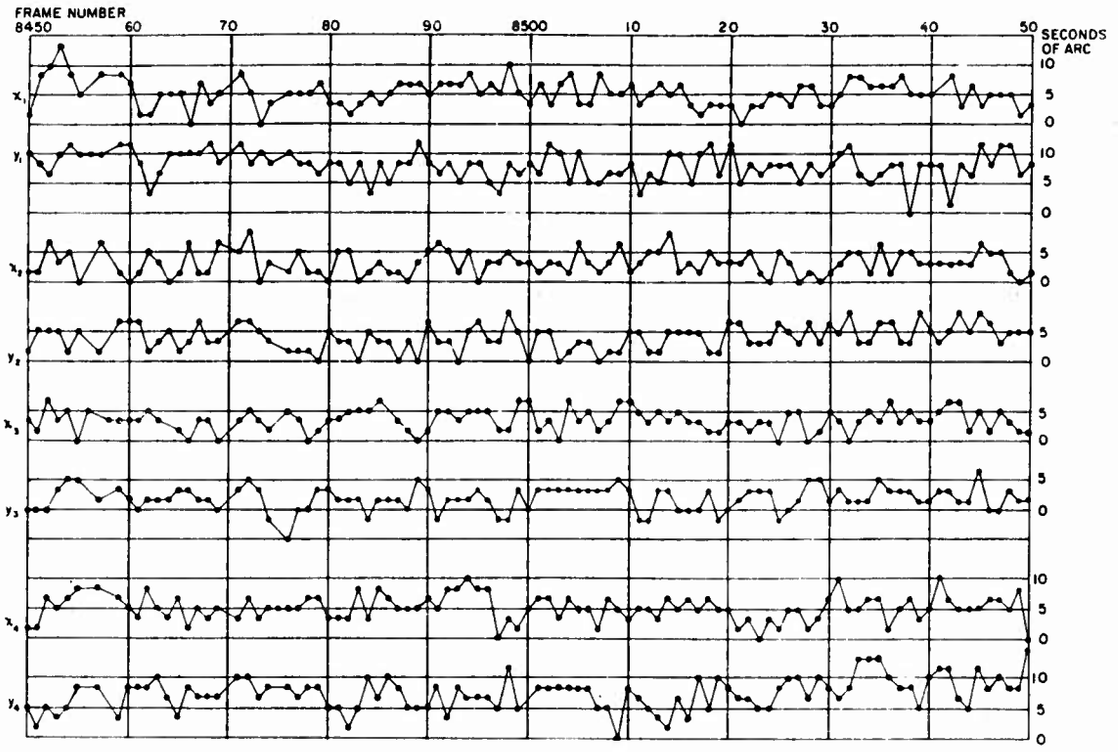

FIG. 23. Frame by Frame Coordinates of the Centers of Disks 1, 2, 3, and 4 Shown in Seconds of Arc Vs Frame Number.

The apparent displacement of the image of a disk is the vector sum of the displacements caused by the above three factors. In the absence of fiducial marks on the film that are independent of camera movement*, the displacements caused by heat waves are separable from the displacements caused by camera movement only by a mathematical procedure which is based upon the fact that the displacements due to camera movement affect the images of all four disks equally.

It is evident that over a period of time long enough to contain many displacements of all types of the image of a disk, the mean location of the center of the disk will be the true location of its center, which may also be called its centroid of motion. Thus the mean coordinates of the center of the disk are the coordinates of the point from which to measure each displacement.

*Subsequent to the initiation of this study, a device for providing such marks was developed. It consists of a prism, fixed to the camera mount, which directs into the camera lens a beam of parallel light originated by a collimator based on the ground near the camera. The target in the collimator consists of the fiducial marks.

The mean X and Y coordinates of each disk are:

$$\left.\begin{aligned} \bar{X}_1 &= \frac{1}{n}\sum_{i=1}^{n} X_{1_i} & \bar{Y}_1 &= \frac{1}{n}\sum_{i=1}^{n} Y_{1_i} \\ \bar{X}_2 &= \frac{1}{n}\sum X_{2_i} & \bar{Y}_2 &= \frac{1}{n}\sum Y_{2_i} \\ \bar{X}_3 &= \frac{1}{n}\sum X_{3_i} & \bar{Y}_3 &= \frac{1}{n}\sum Y_{3_i} \\ \bar{X}_4 &= \frac{1}{n}\sum X_{4_i} & \bar{Y}_4 &= \frac{1}{n}\sum Y_{4_i} \end{aligned}\right\} \quad \text{Eq. (1)}$$

Where n = the number of measures of the coordinates (one measurement per frame)--the same for all four disks; i = the dummy index of the measurements or frame number.

Thus, for each frame the rectangular components of the displacements of the four disks are:

$$\left.\begin{aligned} \Delta X_1 &= X_1 - \bar{X}_1 & \Delta Y_1 &= Y_1 - \bar{Y}_1 \\ \Delta X_2 &= X_2 - \bar{X}_2 & \Delta Y_2 &= Y_2 - \bar{Y}_2 \\ \Delta X_3 &= X_3 - \bar{X}_3 & \Delta Y_3 &= Y_3 - \bar{Y}_3 \\ \Delta X_4 &= X_4 - \bar{X}_4 & \Delta Y_4 &= Y_4 - \bar{Y}_4 \end{aligned}\right\} \quad \text{Eq. (2)}$$

where the X's and Y's are the coordinates of the points measured on the given frame.

Each displacement of a point in an image is the vector sum of the displacements caused by camera movement, by large turbulons, and by small turbulons. Thus for each frame the rectangular components of the displacements of the four disks are the scalar sums:

$$\left.\begin{aligned} \Delta X_1 &= \Delta X_{1_c} + \Delta X_{1_h} + \Delta X_{1_H} & \Delta Y_1 &= \Delta Y_{1_c} + \Delta Y_{1_h} + \Delta Y_{1_H} \\ \Delta X_2 &= \Delta X_{2_c} + \Delta X_{2_h} + \Delta X_{2_H} & \Delta Y_2 &= \Delta Y_{2_c} + \Delta Y_{2_h} + \Delta Y_{2_H} \\ \Delta X_3 &= \Delta X_{3_c} + \Delta X_{3_h} + \Delta X_{3_H} & \Delta Y_3 &= \Delta Y_{3_c} + \Delta Y_{3_h} + \Delta Y_{3_H} \\ \Delta X_4 &= \Delta X_{4_c} + \Delta X_{4_h} + \Delta X_{4_H} & \Delta Y_4 &= \Delta Y_{4_c} + \Delta Y_{4_h} + \Delta Y_{4_H} \end{aligned}\right\} \text{Eq. (3)}$$

Camera movements affect the images of all four disks equally. So do large turbulons, since they cause a shift in the image of the target as a whole. Thus for any given film frame we have the constant sums:

$$\Delta X_{1_c} + \Delta X_{1_H} = K \qquad \Delta Y_{1_c} + \Delta Y_{1_H} = K^1$$

$$\Delta X_{2_c} + \Delta X_{2_H} = K \qquad \Delta Y_{2_c} + \Delta Y_{2_H} = K^1$$

$$\Delta X_{3_c} + \Delta X_{3_H} = K \qquad \Delta Y_{3_c} + \Delta Y_{3_H} = K^1$$

$$\Delta X_{4_c} + \Delta X_{4_H} = K \qquad \Delta Y_{4_c} + \Delta Y_{4_H} = K^1$$

So that Eq. (3) may be subtracted in pairs and written:

$$\left.\begin{aligned} \Delta X_1 - \Delta X_2 &= \Delta X_{1_h} - \Delta X_{2_h} & \Delta Y_1 - \Delta Y_2 &= \Delta Y_{1_h} - \Delta Y_{2_h} \\ \Delta X_1 - \Delta X_3 &= \Delta X_{1_h} - \Delta X_{3_h} & \Delta Y_1 - \Delta Y_3 &= \Delta Y_{1_h} - \Delta Y_{3_h} \\ \Delta X_1 - \Delta X_4 &= \Delta X_{1_h} - \Delta X_{4_h} & \Delta Y_1 - \Delta Y_4 &= \Delta Y_{1_h} - \Delta Y_{4_h} \end{aligned}\right\} \text{Eq. (4)}$$

In each set of equations in Eq. (4) there are three equations in four unknowns, viz., ΔX_{1_h}, ΔX_{2_h}, ΔX_{3_h}, ΔX_{4_h} and ΔY_{1_h}, ΔY_{2_h}, ΔY_{3_h}, ΔY_{4_h}; hence any solution must contain an unknown quantity. If one of these unknowns in each set could be eliminated, however, the set could be

solved for the other three unknowns in terms of the displacement components ΔX_1, ΔX_2, ΔX_3, ΔX_4 and ΔY_1, ΔY_2, ΔY_3, ΔY_4. These are the displacements which are measured on the film.

Now the effect of small turbulons is to cause displacements of relatively small areas of the image. Since these displacements are, in general, different from point to point on the image, for each frame as well as for successive frames, there is a remapping of the points from frame to frame, i.e., there is a distortion. Since distortion is the result of pointwise differences in the displacements, some means of quantifying the overall displacement differences for each frame would be a measure of the distortion caused by small turbulons at the instant represented by the film frame. This will now be developed.

The measure of distortion caused by small turbulons in a given frame (which is applicable to all frames) is therefore the displacement of each point on the image relative to the displacement of a reference point on the image--which is standard for all frames--integrated and averaged over all the points on the image.

The difference between the absolute displacement of a given image point and the absolute displacement of a reference point, for a given frame, will be called the relative displacement of the point for that frame. Any point may be taken as the reference point. Let us select the center of Disk No. 1 for this purpose.

Since the displacements of points on the image for each frame due to small turbulons are referred to the displacement of Point No. 1, this is the same as taking the displacement of Point No. 1 due to small turbulons to be zero for the given frame, i.e., $X_{1_h} = 0$ and $Y_{1_h} = 0$. Stated another way, the displacement of Point No. 1 in a given frame is taken as the zero of an X-displacement scale for that frame, and the Y displacement of Point No. 1 is taken as the zero of a Y-displacement scale. Thus, Eq. (4) becomes:

$$\left.\begin{aligned} \Delta X_{2_h} &= \Delta X_2 - \Delta X_1 & \Delta Y_{2_h} &= \Delta Y_2 - \Delta Y_1 \\ \Delta X_{3_h} &= \Delta X_3 - \Delta X_1 & \Delta Y_{3_h} &= \Delta Y_3 - \Delta Y_1 \\ \Delta X_{4_h} &= \Delta X_4 - \Delta X_1 & \Delta Y_{4_h} &= \Delta Y_4 - \Delta Y_1 \end{aligned}\right\} \quad \text{Eq. (5)}$$

That is, the displacements due to small turbulons are functions of the net displacements measured on the film.

Relative displacement for a given frame, integrated over all points on the image and averaged, is the complete measure of the distortion of the image by small turbulons for that frame. In this study we will not measure the relative displacement of a continuum of points, but we will measure it for three well-distributed-points--the centers of Disks 2, 3, and 4. Thus, we will obtain only a partial measure of the distortion for each frame, but one that is sufficiently descriptive for our purposes. Integrating the relative displacements of these three points and taking the average, we obtain:

$$\Delta\bar{X}_h = 1/3\ (\Delta X_{2_h} + \Delta X_{3_h} + \Delta X_{4_h}) \text{ and } \Delta\bar{Y}_h = 1/3\ (\Delta Y_{2_h} + \Delta Y_{3_h} + \Delta Y_{4_h}) \quad \text{Eq. (6)}$$

which is the measure of distortion of the image at the instant of time represented by the frame, to the accuracy permitted by selecting three points out of a continuum of points.

It might be well to point out that setting to zero the absolute displacement of the reference point due to small turbulons is legitimate, since it is consistent with the fact that distortion is a measure of the relative--not the absolute--displacement of image points, and absolute displacements must have a common reference such as zero if they are to be compared with each other for the purpose of determining relative displacements.

Figure 24 plots the Δ's given by the left side of Eq. (5) vs frame number. Figure 25 plots $\Delta\bar{X}_h$ and $\Delta\bar{Y}_h$ vs frame number, as determined from Eq. (6).

Approximately 100 sets of measures--a set is four measures per frame--are processed as described by Eqs. (1) through (6), and the relations expressed by the latter are plotted in Fig. 25. Figure 25 thus indicates the degree of image distortion vs time. In Figs. 23, 24 and 25, the frame numbers are shown along the tops of the graphs.

Figures 26, 27, and 28 are rectangular plots of the X and Y displacements of the centroid of the images of Disks 2, 3, and 4 with respect to Disk 1. The plotted points are labeled with the last two digits of the corresponding frame numbers. The points are connected in succession by straight lines which are dotted in the several cases where an observation is missing. The origin of each graph is the mean position of the centroid whose motion is shown on the graph. (Units in Figs. 26, 27, and 28 are plotted in seconds of arc in both the X and Y directions.)

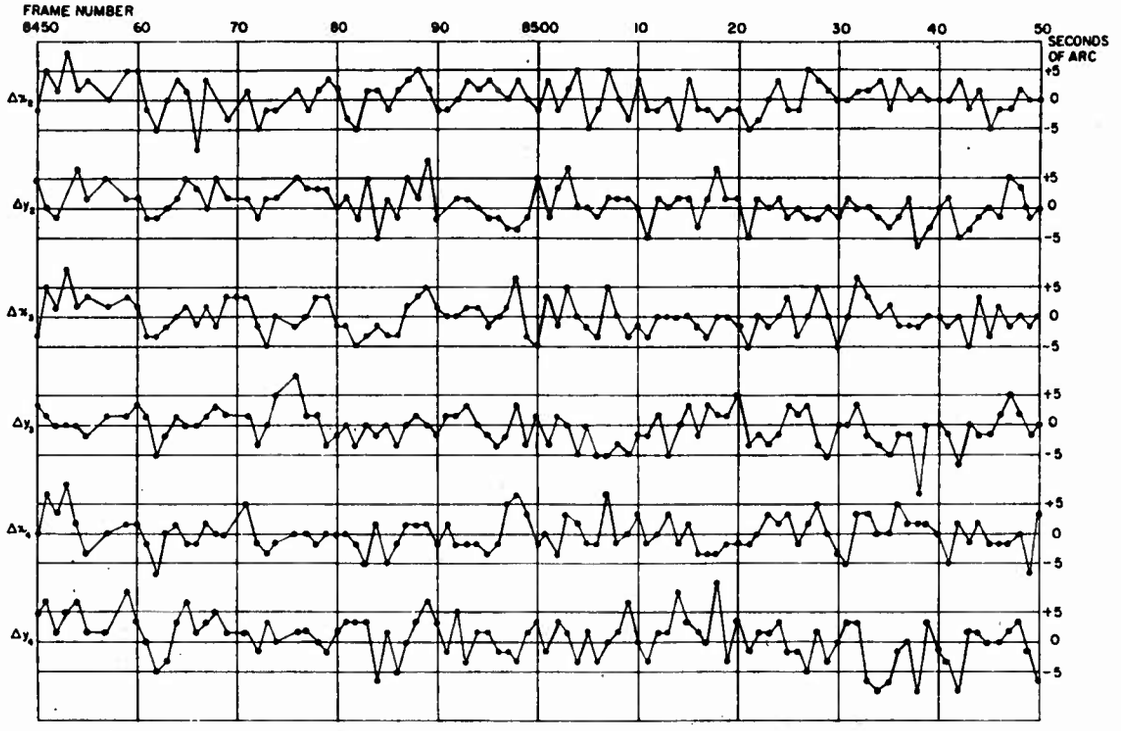

FIG. 24. Frame by Frame Plot of Displacements in X and Y Directions of Disks 2, 3, and 4 Relative to Disk 1, Plotted in Seconds of Arc Vs Frame Number.

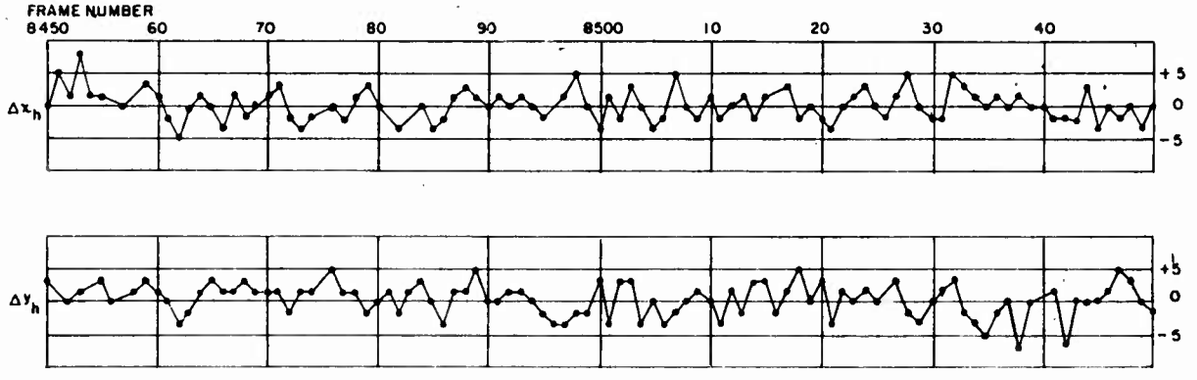

FIG. 25. X and Y Image Distortions Plotted Frame by Frame in Seconds of Arc Vs Frame Number.

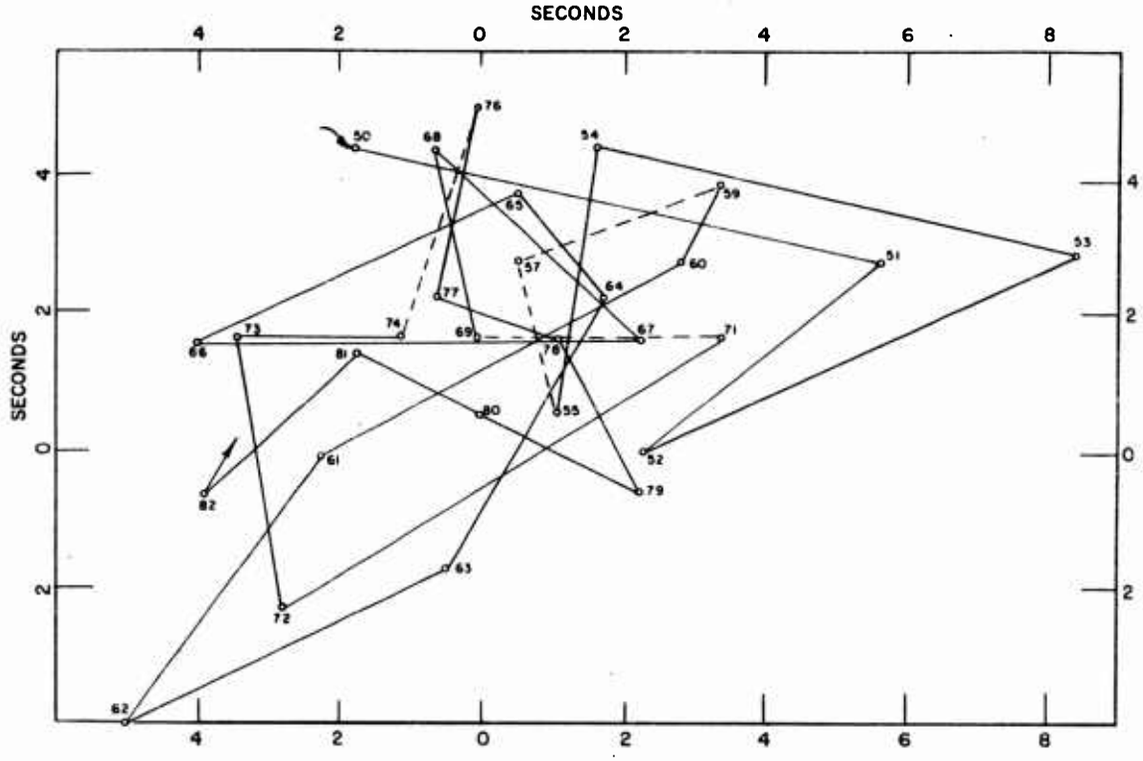

FIG. 26. Rectangular Plot of $\Delta\bar{X}_h$ and $\Delta\bar{Y}_h$ for Frames 8450-8482. Units are plotted in seconds of arc in both the X and Y directions.

The results thus obtained indicate clearly that, even with good atmospheric conditions, the position of an object as determined from photographic records may be in error by quite a few seconds of arc. In this case these errors are about ±5 seconds for a path of 500 feet length running essentially parallel to the ground at a height of five feet. The distribution of density of observations for zones of radius R about the centroid for one disk is shown in Fig. 29. The histogram resembles a chi-square distribution curve, as might be expected. This conformity seems excellent evidence of randomness for these errors. It does not however identify turbulons as the cause. Dimensional instability in photographic film, for example, may be the significant random contributer to these errors. Dimensional instability in the film might be expected to introduce image displacements in the range 10-20 microns which would correspond to a directional error of ±3 seconds for the 48-inch lens used in this test.

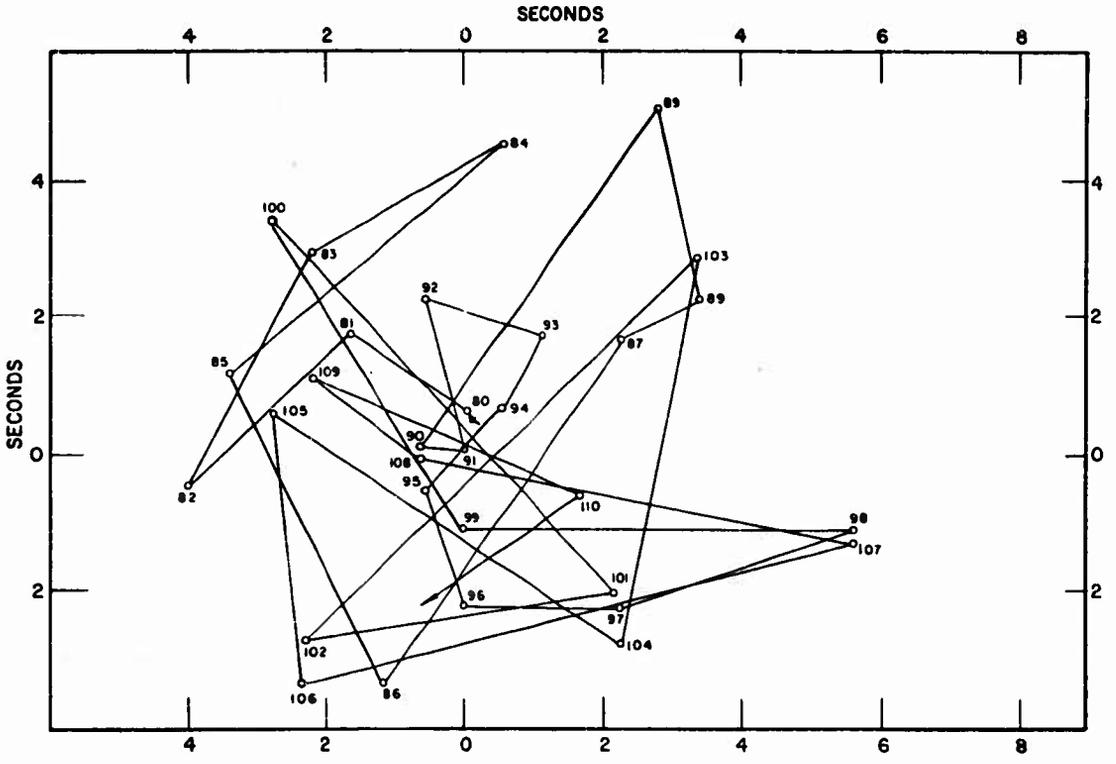

FIG. 27. Rectangular Plot of $\Delta\bar{X}_h$ and $\Delta\bar{Y}_h$ for Frames 8480-8510. Units are plotted in seconds of arc in both X and Y directions.

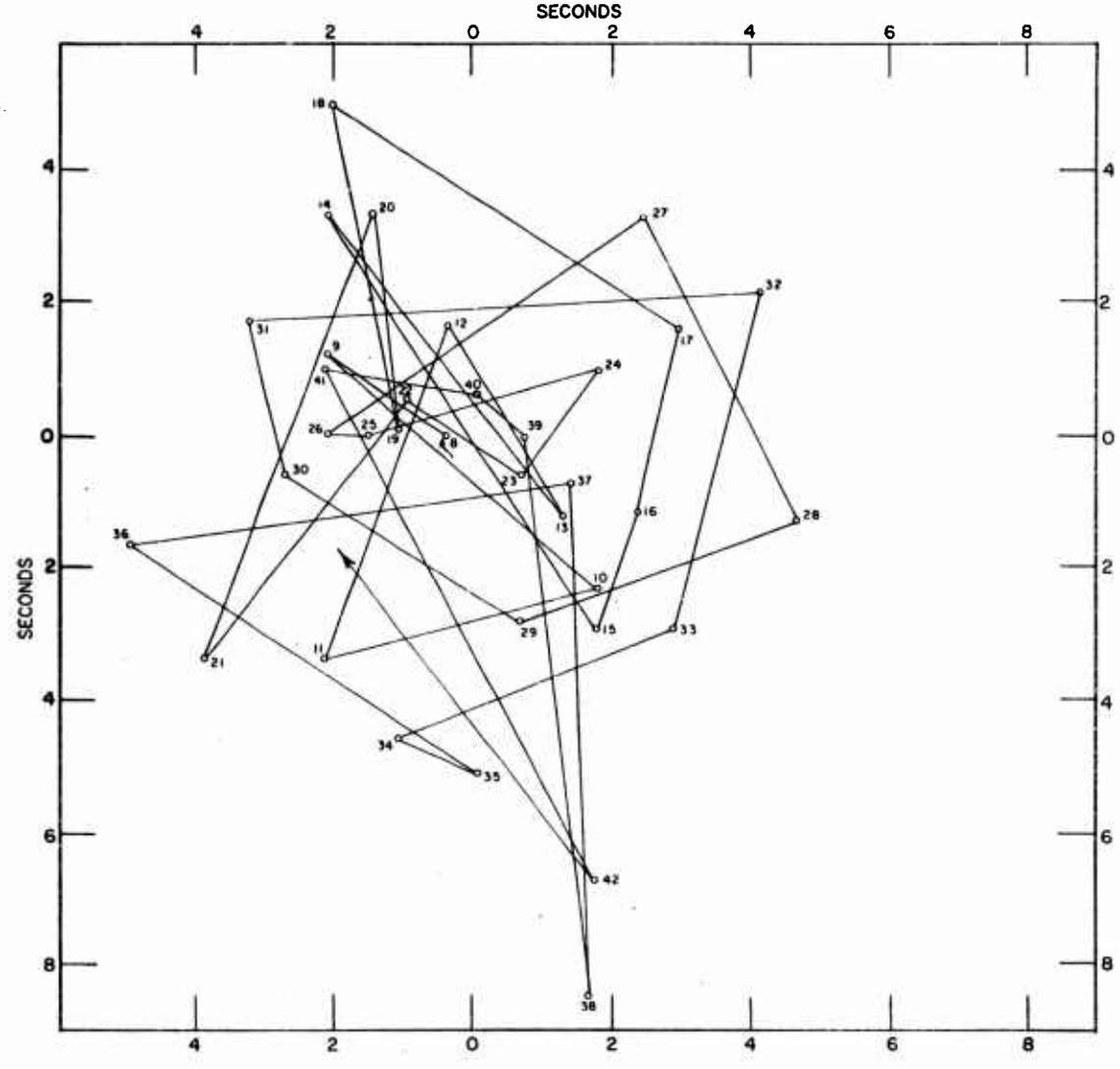

FIG. 28. Rectangular Plot of $\Delta\bar{X}_h$ and $\Delta\bar{Y}_h$ for Frames 8508-8542. Units are plotted in seconds of arc in both the X and Y directions.

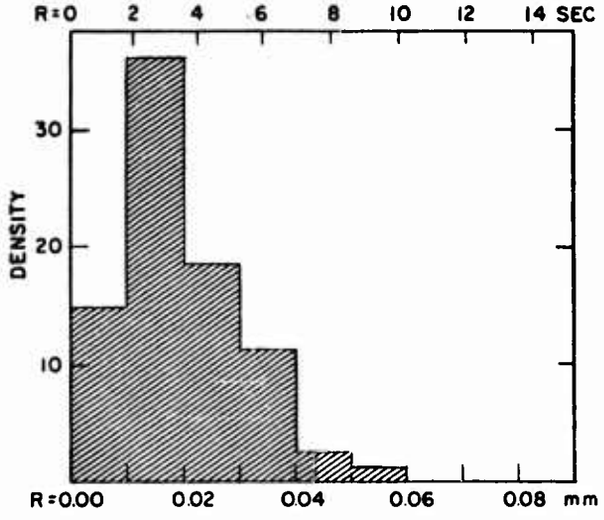

FIG. 29. Density Distribution of Observations for Zones of Radius R.

A set of observations similar to those discussed in the foregoing paragraphs was made later on the same day when the seeing had become poor. These data are shown in Figs. 30-34, and require little comment except that the change in scale from that used in the first series should be noted in Figs. 32, 33, and 34. The more pronounced erratic motion of the photographic images under poor seeing conditions is well brought out by the charts. These poor seeing conditions are by no means worst seeing conditions. Motions of the images that were much more violent have been observed.

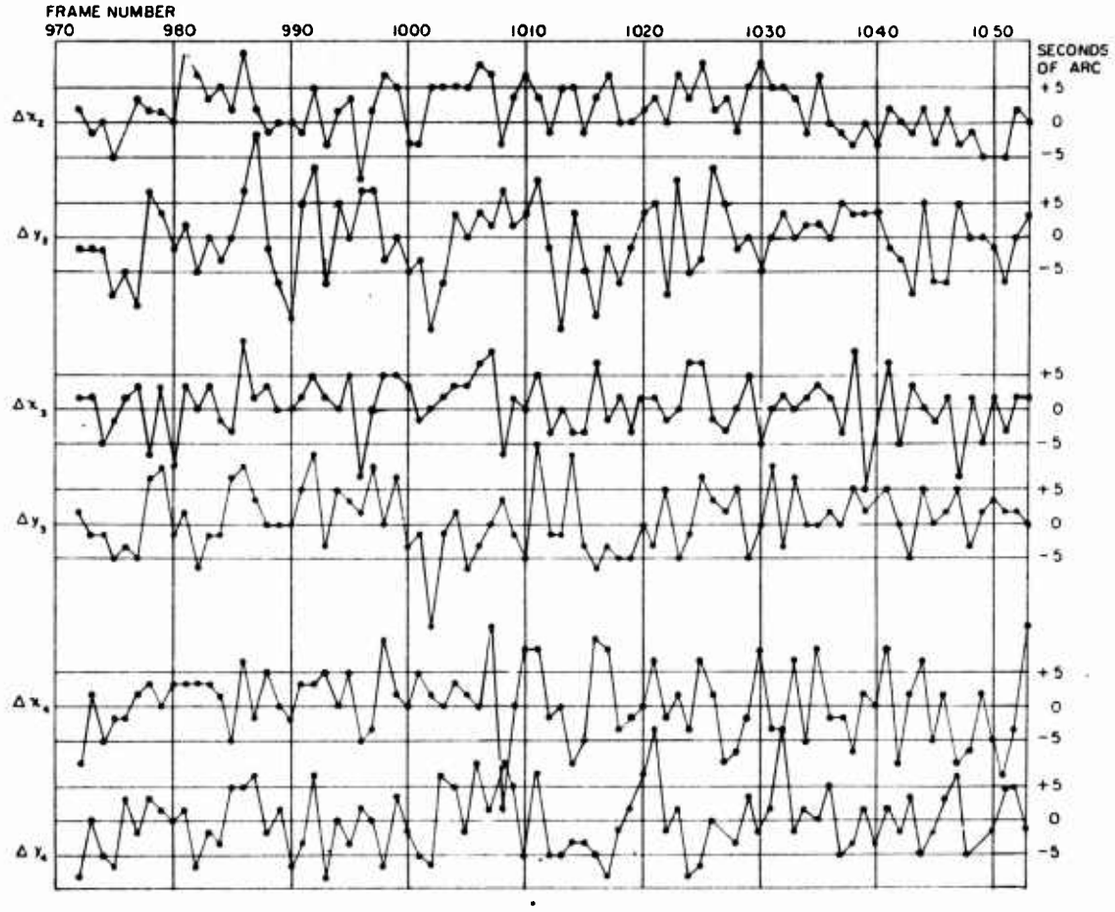

FIG. 30. Frame by Frame Plot of Displacements in X and Y Directions of Disks 2, 3, and 4 Relative to Disk 1. These curves are for poor seeing conditions and correspond to Fig. 24 which was plotted from data taken under good seeing conditions.

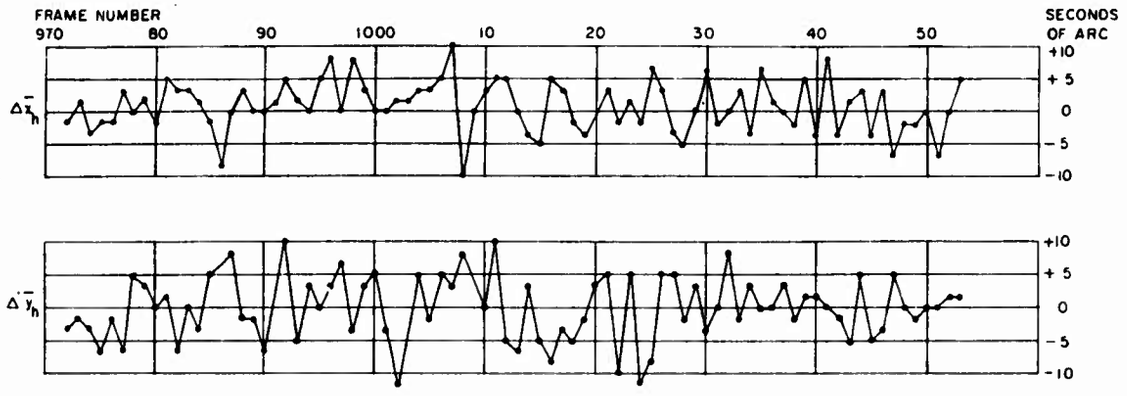

FIG. 31. Frame by Frame Plot of the X and Y Distortions of the Image Under Poor Seeing Conditions. This contrasts with Fig. 25 which was plotted from data obtained under good seeing conditions.

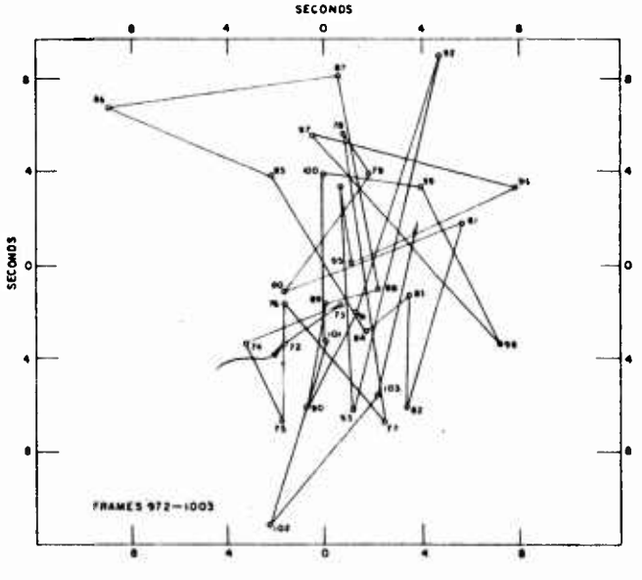

FIG. 32. Rectangular Plot of $\Delta\bar{X}_n$ and $\Delta\bar{Y}_h$ Frames 972-1003 (Poor Seeing Conditions).

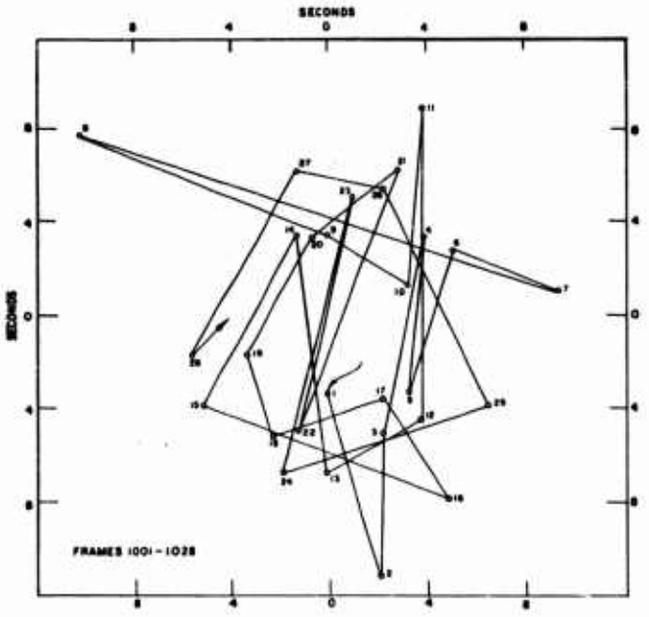

FIG. 33. Rectangular Plot of $\Delta\bar{X}_h$ and $\Delta\bar{Y}_h$ for Frames 1001-1028 (Poor Seeing Conditions.

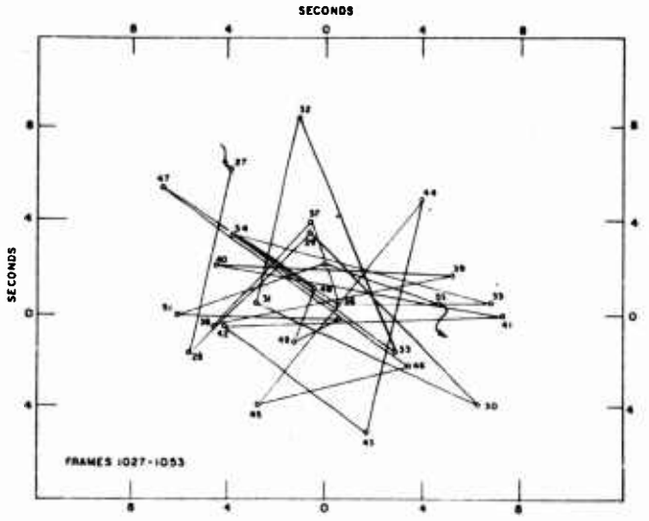

FIG. 34. Rectangular Plot of $\Delta\bar{X}_h$ and $\Delta\bar{Y}_h$ for Frames 1027-1053 (Poor Seeing Conditions).

Appendix C

EXPERIMENTAL DETAILS OF GROUND COVER STUDIES

The data from a year-long series of observations taken at approximately two-week intervals to determine the resolution of targets at various camera heights and target distances, were summarized on 6,500 IBM cards. Six hundred of these cards, randomly selected, were used in a multitude linear regression analysis* to obtain a relationship between the observed photographic resolution and the conditions of the exposure. The derived equation is:

$$Y' = 31.913 - 0.581X_1 + 0.219X_2 - 0.035X_3 - 0.169X_4 \qquad \text{Eq. (7)}$$

Where

Y' is the calculated value of resolution in lines/mm

X_1 is the target distance in feet divided by 250

X_2 is the camera height in feet

X_3 is the net convective remainder** in $BTU/hr/ft^2$

X_4 is the temperature in degrees F

Since variation in the net convective remainder (NCR) over the observed range may produce a significant effect on photographic resolution, the question to be answered in this experiment is: What happens to the NCR when various ground cover modifications are applied? Any change in the NCR would in turn mean a change in the resolution according to the derived equation.

The method selected for the preliminary evaluation of the effect of ground cover modification was to set up two net radiant exchange radiometers (one of them for control purposes), with their associated ground conduction transducers. This setup was used to measure the change in radiation and ground conduction resulting from the application of various ground cover treatments.

---

* The multiple linear regression analysis was made by James R. Harvey of the Assessment Division, Test Department, NOTS.

** The net convective remainder is defined on page 24.

Of the total solar energy incident upon the surface of the earth, E_t, a portion is reflected from the surface and a portion is absorbed by the ground. The energy re-radiated from the ground, combined with that which is reflected, is called E_r, and strikes the underside of the transducer in the net exchange radiometer. Thus the net exchange radiometer measures $E_t - E_r$. A transducer under the surface of the ground measures the energy being conducted into the earth. The difference between the net exchange above the earth and the ground conduction is considered to be available to produce convective heating of the air, with consequent turbulence.

EXPERIMENTAL CONDITIONS

Two net radiant exchange radiometers, with their associated ground conduction transducers, were set up to receive, as closely as practicable, identical solar radiation. After the instruments had been in place for a while, the ground cover was modified in the vicinity of one of the instruments. Instruments were also set up to record wind velocity and ambient air temperature.

The first two tests, one involving application of lime and the other sprinkling of water, were conducted on bare ground. For the first test thirty pounds of dry lime were applied to a circular area 24 feet in diameter. For the second test, water was sprinkled on a similar area at a rate of $1\frac{1}{2}$ gallons per minute for a period of 20 minutes. The location of instruments used is shown in Fig. 35. The third test was conducted on a lawn adjacent to a plot of bare ground.

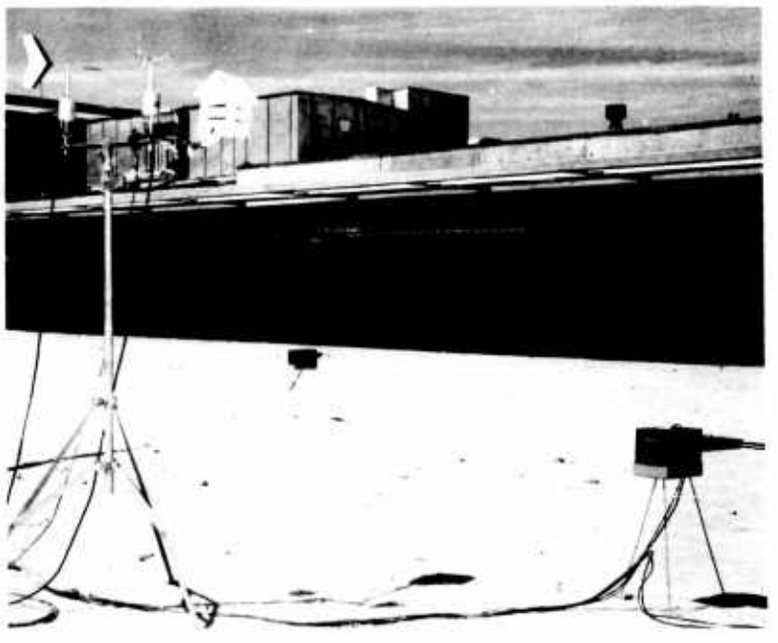

FIG. 35. Area Used in Experimental Determination of the Effect of Spread Lime on Net Radiation.

A transducer similar to the one used above ground, but with no air blower, was placed about 3/16 inch below the surface of the ground to measure ground heat conduction.

Wind velocity (which consists of speed and direction) was obtained with a Beckman-Whitley climate-survey wind speed and direction recorder, Model 170-2. A three-cup anemometer and wind vane were mounted on a stand about six feet above the ground (see Fig. 36).

Ambient air temperature was measured by recording the output of two copper-constantan thermocouples. One thermocouple was mounted inside a miniature thermoscreen about 6 feet above ground level (Fig. 36), and the other was placed inside a white-painted aluminum tube on the intake of a squirrel-cage blower.

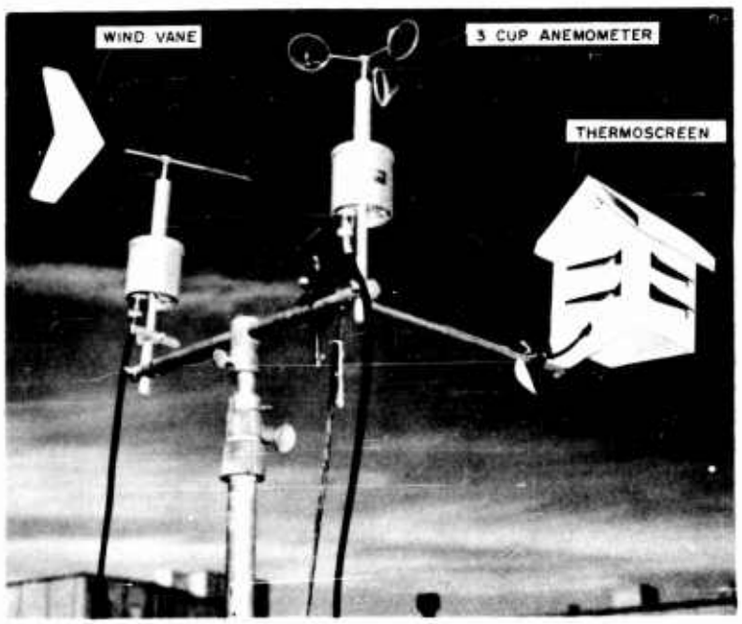

FIG. 36. Beckman-Whitley Wind Velocity Instrument.

DATA REDUCTION TECHNIQUES

The temperature of the transducers and radiometers, in degrees F, the output of the transducers and radiometers in millivolts, and the ambient air temperature were recorded on two Brown Electronik recorders.

For each radiometer and transducer there is a corresponding constant in BTU/hr/ft^2/mv. This constant, K, and a calibrated, temperature-dependent, multiplying factor, F_t, are furnished by the manufacturer of the net exchange radiometers.

The NCR is the product of $K \cdot F_t \cdot mv$ for the transducer, subtracted from the product of $K \cdot F_t \cdot mv$ for the corresponding radiometer. The values needed to compute the NCR were read from the data at 15-minute intervals. The interval was reduced to one minute during periods of special interest.

Wind speed and wind direction were recorded on Esterline-Angus graphic ammeters. The data were then read and plotted over intervals of one minute.

RESULTS

Ambient air temperature during each of the three tests is shown in Fig. 37. The most promising test was the one conducted with lime. Upon application of the lime the NCR for this area dropped almost immediately to approximately half the value of the NCR for its corresponding control area, as shown in Fig. 38, which is a history of the time of lime application for the entire lime-spreading experiment. Figure 39(a) is a portion of the time history sampled every minute, and Fig. 39(b) shows the calculated theoretical effect on the drop in NCR on image resolution using Eq. (7) and selecting 1,000 feet for the target distance and 6 feet for the camera height. The calculated resolution for the limed area was approximately three lines/mm greater than the calculated resolution of its control area. According to the equation, the calculated resolution would always be 3 lines/mm better for a limed area, regardless of target distance or camera height. The significance of a 3-line/mm increase diminishes as the resolution increases. However, with exposure conditions that exist on ranges at NOTS, which often result in low values of photographic resolution, an increase of 3 lines/mm would often improve the information content of a photographic record considerably.

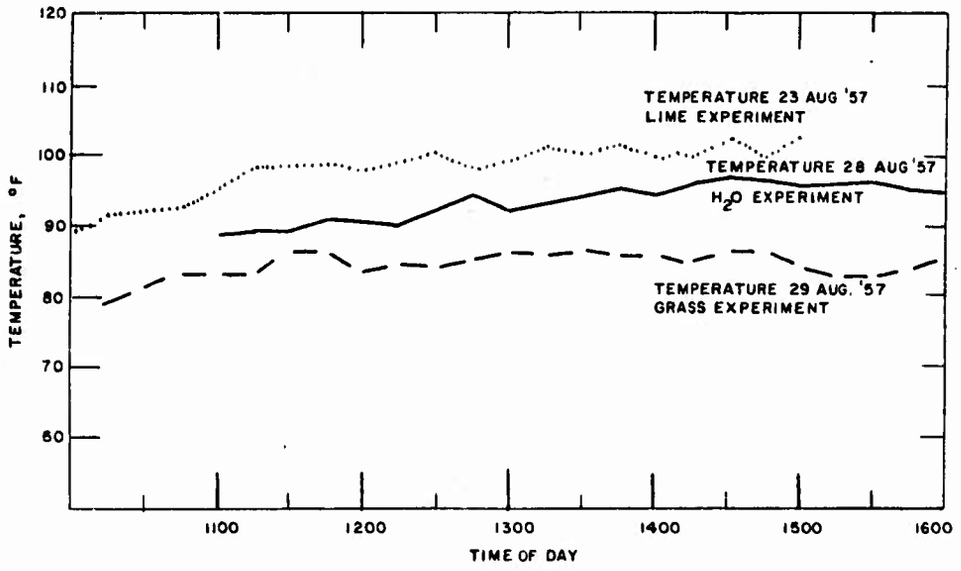

FIG. 37. Record of Ambient Air Temperature During Three Tests.

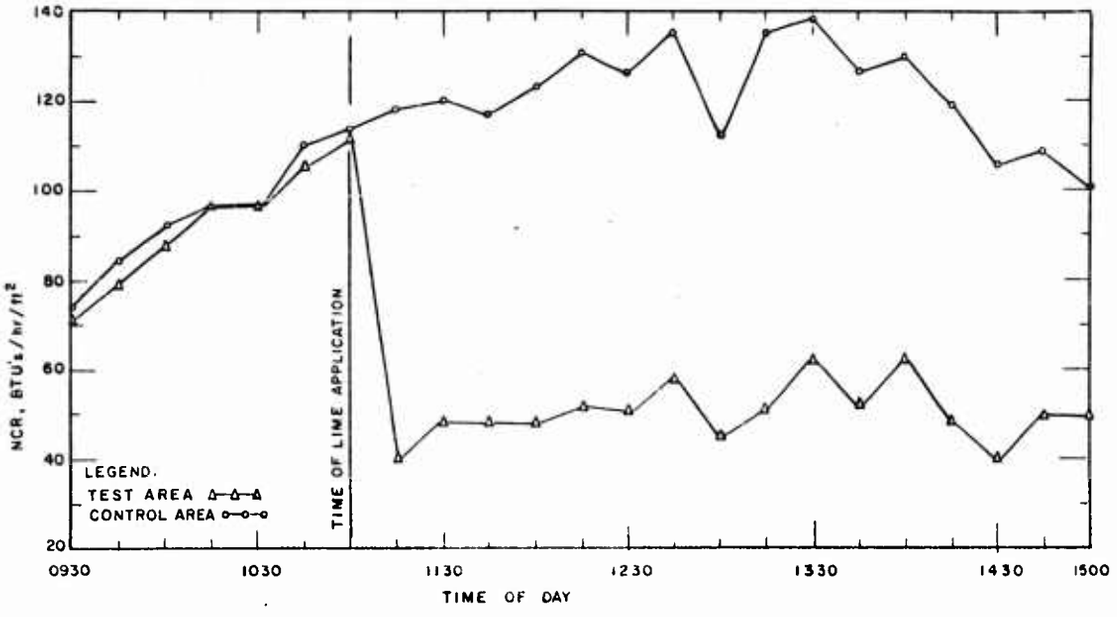

FIG. 38. Record of NCR During Lime Test.

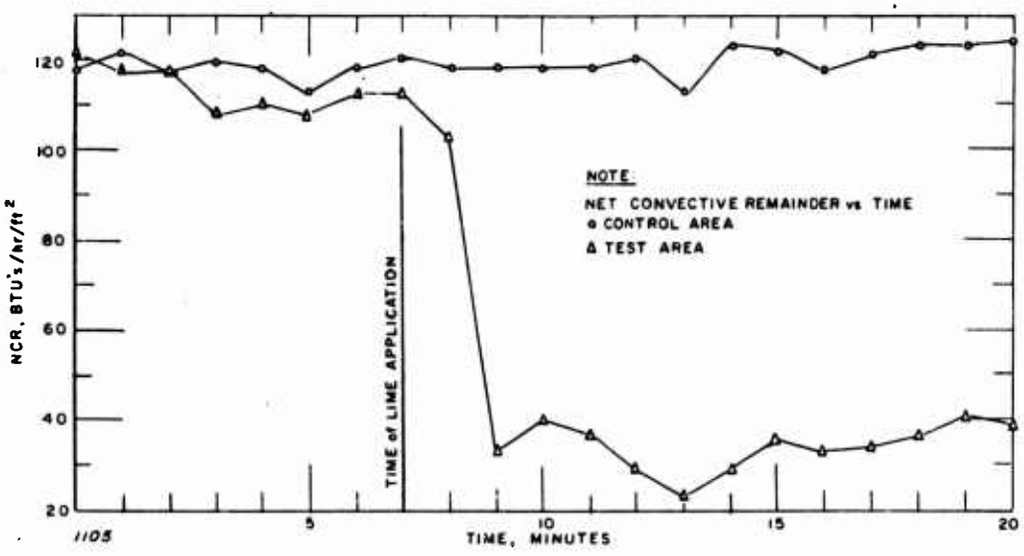

FIG. 39(a). Partial Record of NCR During Lime Test From Data Taken at One-Minute Intervals. The abrupt drop in NCR is shown to occur within two minutes of application of lime to test area.

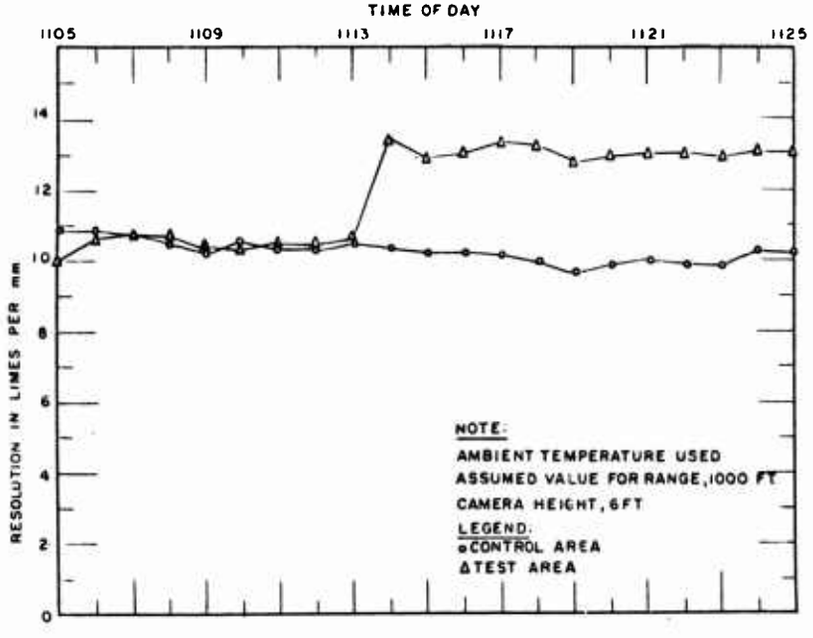

FIG. 39(b). Theoretical Effect of the Drop in NCR on Image Resolution.

It was noted earlier that the interval for sampling the data was decreased during periods of special interest. The NCR was plotted to show the effect of the passing of thin high clouds, and the passing of a dust devil (whirlwind). The dust devil, traveling toward the east, stopped for a short time over the area covered with lime. It gathered lime, which rose in a column about 60 feet in the air, then continued eastward. There were no effects on the NCR of the limed area after the dust devil had passed; however, during the passage of both the clouds and the dust devil the NCR of the test area and that of the control area dropped. The dust devil produced the largest drop. The effects of both are shown in Fig. 40.

The application of water to the test area increased the computed NCR approximately 60 BTU/hr/ft^2 over the NCR of its control area; however, after several hours of evaporation the NCR of the test area again approached that of the control area (Fig. 41). The NCR was originally computed by assuming that any energy which wasn't reflected or re-radiated or conducted into the ground is available to produce convective heating. Evaporation near the surface would dissipate energy which formerly was available for ground heat conduction or reflection or re-radiation. A more accurate value of the NCR could be obtained by adding another term to the equation for the NCR, making it: NCR = $(E_t-E_r-E_g-E_e)$ where E_e is the amount of energy dissipated by evaporation. The instrumentation used did not measure E_e, and therefore the water test was considered inconclusive.

The computed NCR of the grass-covered area was approximately 60 BTU/hr/ft^2 greater than that of the control area throughout the test (Fig. 42). However, in this test a part of the incident energy was converted by the grass into energy, which it used for growing. Since the grass area was sprinkled frequently, some energy was lost through evaporation. Thus two more values should be added to the original equation for the NCR, making it NCR = $(E_t-E_r-E_g-E_v-E_e)$, E_e being the energy dissipated by evaporation, and E_v the energy used by the grass for growth. Since neither E_e nor E_v was measured, this test was also considered inconclusive.

In general, temperatures from the blower thermocouple were lower than temperatures from the thermoscreen, indicating some buildup of heat in the thermoscreen. Temperatures shown in Fig. 37 are those obtained in the blower airstream. There seemed to be no correlation between wind velocity and NCR.

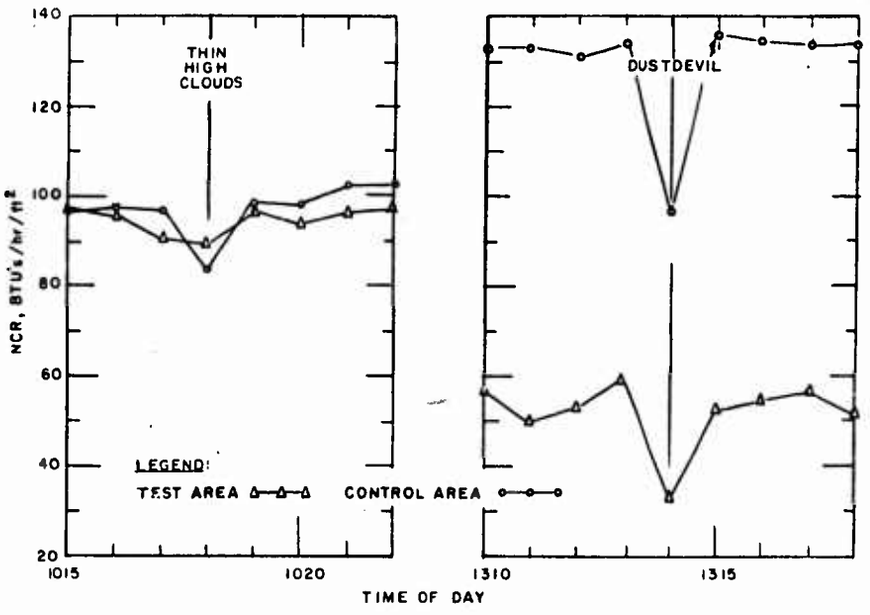

FIG. 40. A Detailed Record of NCR During Passage of Clouds and Dust Devil Over Test Area.

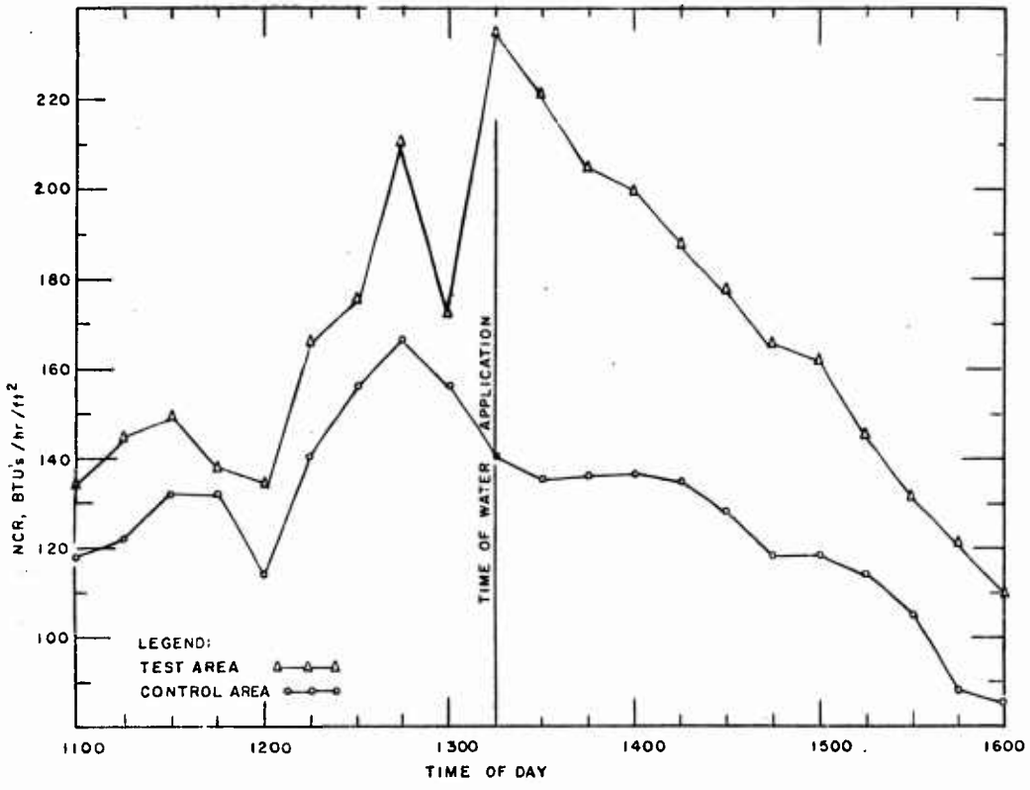

FIG. 41. Record of NCR During Water Test.

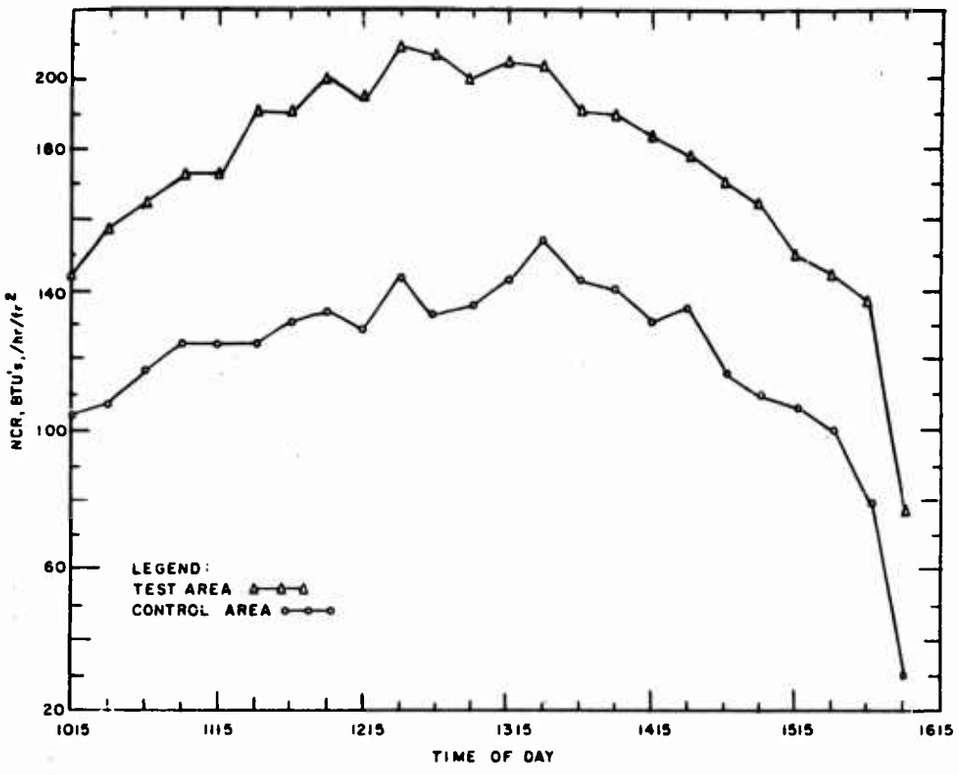

FIG. 42. Record of NCR During Grass Test.

ACKNOWLEDGMENT

The roster of those involved in the planning and execution of an experimental program of the scope and duration covered by this paper is too great to be properly set forth here. Special acknowledgment should be made, however, of the extensive, basic contributions made by the late William H. Christie, under whose direction the program was initiated. Special mention should also be made of Carroll L. Evans, Jr., Lynn L. Lyon, Bruce W. Dorsch, Carl W. Koiner, Paul G. Bauer, Richard G. Brophy, and Bruce R. Morton, Jr., who contributed substantially to the design of the experiments and the apparatus used, and who gathered the data.

BIBLIOGRAPHY

1. Becker, R. A. "Effects of Atmospheric Turbulence on Optical Instrumentation," I.R.E. Transactions on Military Electronics, Vol. MIL-5, No. 4 (October 1961), pp. 352-356.

2. Boston University Optical Research Laboratory. The Deterioration of Image Quality Caused by a Heated Air Window Defrosting System, by John Watson. Boston, Mass., 27 January 1950. (Tech Note No. 60.)

3. ------. A Collection of Graphs Concerning Atmospheric Transmission, Natural Illumination and Reflectance of Terrain, by R. E. Dillon. Boston, Mass., 1 July 1952. (Tech Note No. 87.)

4. Boston University Physical Research Laboratories. Final Report, An Investigation of Photographic Techniques for the Recording of Missile Flight. Boston, Mass., May 1957.

5. Brooks, F. A. "Atmospheric Radiation and Its Reflection from the Ground," J METEOROL, Vol. 9, No. 1 (February 1952), pp. 41-52.

6. Cone, C. D. "Thermal Soaring Birds," AMERICAN SCIENTIST J, Vol. 50, No. 1 (March 1962), pp. 180-209.

7. Cornell University. Final Report, Research Investigations into Factors Affecting Long Range Photography. Ithaca, New York, August 1954.

8. Gaviola, E. "On Seeing, Fine Structure of Stellar Images, and Inversion Layer Spectra," ASTRON J, No. 1178 (1949), pp. 155-161.

9. Gerhardt, J. R., and others. "Fluctuations of Atmospheric Temperature as a Measure of the Heat and Intensity of Turbulence Near the Earth's Surface," J METEOROL, Vol. 9, No. 5 (October 1952), pp. 299-310.

10. Gugenheim Aeronautical Laboratory. Investigation of Atmospheric Turbulence, by H. J. Stewart and P. B. MacCready, Jr. California Institute of Technology, Pasadena, Calif., May 1952.

11. Guild, W. R. "Note on the Heat Transfer at the Soil Surface," J METEOROL, Vol. 7, No. 2 (April 1950), pp. 140-144.

12. Hardy, Arthur C. "Atmospheric Limitations on the Performance of Telescopes," OPT SOC AM, J, Vol 36, No. 5 (May 1946), pp. 283-7.

13. Hofleit, Dorrit. "Seeing," SKY AND TELESCOPE, Vol 9, No. 3 (January 1950), pp. 57-8.

14. Hofleit, Dorrit. "Seeing," SKY AND TELESCOPE, Vol. 9, No. 4 (February 1950), pp. 88-9.

15. Jehn, K. H., and J. R. Gerhardt. "Surface Atmospheric Heat Flux Analysis on the Littau Model," J METEOROL, Vol. 10, No. 1 (February 1953), pp. 10-16.

16. Lamar, E. S., and others. "Size, Shape, and Contrast in Detection of Targets by Daylight Vision," OPT SOC AM, J, Vol. 38, No. 9 (September 1948), pp. 741-55.

17. Library of Congress, Reference Department. Visibility, a Bibliography, by M. Leikind and J. Weiner. Washington, D. C., July 1952. (Ref. Z7144, O6U5).

18. Middleton, W. E. K. Vision Through the Atmosphere. Toronto, Canada, University of Toronto Press, 1952. 250 pp.

19. Naval Research Laboratory. Influence of Atmosphere on Optical Resolution in a Typical Nevada Tunnel, by A. G. Rockman. Washington, D. C., March 31, 1960. (Report No. 5459.)

20. New York University, College of Engineering Research Division. Experimental Studies of Small Scale Turbulence, by James E. Miller, Alfred K. Blackadar, Wan-Cheng Chiu, and Warren A. Dryden. New York, N. Y., August 1955.

21. Riggs, L. A., C. G. Muller, C. H. Graham, and F. A. Mote. "Photographic Measurement of Atmospheric Boil," OPT SOC AM, J, Vol 37, No. 6 (June 1947), pp. 415-20.

22. U. S. Naval Ordnance Test Station. An Analysis of Atmospheric Data at the Naval Ordnance Test Station, by D. L. Farnham, I. C. Vercy, and Q. S. Dalton. China Lake, Calif., NOTS, 15 January 1955. (NAVORD Report 3391, NOTS 973.)

23. ------. Atmospheric Refraction in the Visible Spectrum, by R. J. Stirton. China Lake, Calif., NOTS, 1 December 1959. (NAVORD Report 6614, NOTS TP 2357.)

24. ------. Effect of Solar Radiation on the Temperatures in Metal Plates with Various Surface Finishes, by C. M. Arney and C. L. Evans, Jr., China Lake, Calif., NOTS, May 1953. (NAVORD Report 6401, NOTS 2097.)

25. ------. General Photographic Instrumentation Plan for SNORT, by E. E. Green, R. W. Herman, and D. S. Bowman. China Lake, Calif., NOTS, 27 March 1952. (NOTS TM 242.)

26. ------. Meteorological Instrumentation and Techniques. by Paul H. Miller. China Lake, Calif., NOTS. (Lecture.)

27. ------. Optimum Azimuth for the Exterior Ballistic Research Range and Optimum Conditions for Photography and Other Open Range Ballistic Observations, by Gordon W. Wares. China Lake, Calif., NOTS, 1 July 1947. (NOTS TM No. SBE-15.)

28. ------. Reproducibility of Readings of Film From Askania Cinetheodolite, by John Titus and Paul Peach. China Lake, Calif., NOTS, June 1953. (NOTS TM 285.)

29. ------. A Study of Heat Waves, by William C. Ward. China Lake, Calif., NOTS, 27 January 1948. (NOTS TM OMM-2.)

30. ------. A Study of Upper Air Temperatures at the Naval Ordnance Test Station, by Paul H. Miller. China Lake, Calif., NOTS, 15 June 1956. (NAVORD Report 5256, NOTS 1463.)

31. ------. Temperature Measurements from 10 Feet Above to 10 Feet Below the Earth's Surface, by W. C. Ward. China Lake, Calif., NOTS, April 1952. (NOTS TM-243.)

32. ------. Thermal and Air Turbulence Effects on the Alignment of Photographic Resolution of a Sheltered Askania Cinetheodolite, by C. L. Evans. China Lake, Calif., NOTS, 1 December 1955. (NAVORD Report 5250, NOTS 1452.)

33. Washer, Francis E., and Helen Brubaker Williams. "Precision of Telescope Pointing for Outdoor Targets," OPT SOC AM, J, Vol. 36, No. 7, pp. 400-411.

34. Wood, Robert W. Physical Optics. New York, Macmillan Co., 1934. 846 pp.

INITIAL DISTRIBUTION

12 Chief, Bureau of Naval Weapons
- Steering Committee Member, IRIG (1)
- DLI-31 (2)
- FF (1)
- R-362 (1)
- RM-2 (1)
- RMGA-41 (1)
- RRRE-3 (1)
- RMWC-521 (1)
- RMWC-533 (1)
- RTPA-2 (1)
- RTSA-21 (1)

2 Chief of Naval Research
- Member, Meteorological Working Group, IRIG (1)
- Code 104 (1)

2 Naval Air Development Center, Johnsville

6 Naval Missile Center, Point Mugu
- Members, Optical Systems Working Group, IRIG (2)
- Member, Photographic Processing Working Group, IRIG (1)
- Members, Meteorological Working Group, IRIG (2)
- Technical Library (1)

2 Naval Weapons Services Office

4 Army Ordnance Missile Command, Redstone Arsenal (Technical Library)

4 Redstone Arsenal
- Member, Meteorological Working Group, IRIG (1)
- Members, Optical Systems Working Group, IRIG (2)
- Member, Photographic Processing Working Group, IRIG (1)

1 Signal Corps Engineering Laboratories, Fort Monmouth (Technical Document Center)

9 White Sands Missile Range
- Secretariat, IRIG (1)
- Members, Optical Systems Working Group, IRIG (2)
- Members, Photographic Processing Working Group, IRIG (1)
- Members, Meteorological Working Group, IRIG (2)
- Technical Library (3)

6 Air Force Flight Test Center, Edwards Air Force Base
- Steering Committee Member, IRIG (1)
- Members, Optical Systems Working Group, IRIG (2)
- Members, Photographic Processing Working Group, IRIG (2)
- Member, Geodetic Working Group, IRIG (1)

1 Air Force Missile Development Center, Holloman Air Force Base

7 Air Force Missile Test Center, Patrick Air Force Base
- Steering Committee Member, IRIG (1)
- Members, Optical Systems Working Group, IRIG (2)
- Members, Photographic Processing Working Group, IRIG (2)
- Members, Meteorological Working Group, IRIG (2)

NOTS CL 456 (9/62) 2C

ABSTRACT CARD

U. S. Naval Ordnance Test Station
Summary of Investigations of Heat-Wave Effects on Photographic Images, compiled by Richard B. Walton. China Lake, Calif., NOTS, October 1962. 54 pp. (NAVWEPS Report 7773, NOTS TP 2754), UNCLASSIFIED.

ABSTRACT. A comprehensive report of a year's data, taken from a special range established at NOTS for study of heat wave problems, is presented. The data include micrometeorological information as well as optical and photographic results obtained at frequent

(Over)
1 card, 4 copies

U. S. Naval Ordnance Test Station
Summary of Investigations of Heat-Wave Effects on Photographic Images, compiled by Richard B. Walton. China Lake, Calif., NOTS, October 1962. 54 pp. (NAVWEPS Report 7773, NOTS TP 2754), UNCLASSIFIED.

ABSTRACT. A comprehensive report of a year's data, taken from a special range established at NOTS for study of heat wave problems, is presented. The data include micrometeorological information as well as optical and photographic results obtained at frequent

(Over)
1 card, 4 copies

U. S. Naval Ordnance Test Station
Summary of Investigations of Heat-Wave Effects on Photographic Images, compiled by Richard B. Walton. China Lake, Calif., NOTS, October 1962. 54 pp. (NAVWEPS Report 7773, NOTS TP 2754), UNCLASSIFIED.

ABSTRACT. A comprehensive report of a year's data, taken from a special range established at NOTS for study of heat wave problems, is presented. The data include micrometeorological information as well as optical and photographic results obtained at frequent

(Over)
1 card, 4 copies

U. S. Naval Ordnance Test Station
Summary of Investigations of Heat-Wave Effects on Photographic Images, compiled by Richard B. Walton. China Lake, Calif., NOTS, October 1962. 54 pp. (NAVWEPS Report 7773, NOTS TP 2754), UNCLASSIFIED.

ABSTRACT. A comprehensive report of a year's data, taken from a special range established at NOTS for study of heat wave problems, is presented. The data include micrometeorological information as well as optical and photographic results obtained at frequent

(Over)
1 card, 4 copies

time intervals at various distances and from several camera elevations.

As a result of multiple correlation analyses of these data three experiments were conducted. Results of these experiments, which demonstrate that it is possible to modify the heat wave problem by application of various ground cover materials, are also presented.

NAVWEPS REPORT 7773

time intervals at various distances and from several camera elevations.

As a result of multiple correlation analyses of these data three experiments were conducted. Results of these experiments, which demonstrate that it is possible to modify the heat wave problem by application of various ground cover materials, are also presented.

NAVWEPS REPORT 7773

time intervals at various distances and from several camera elevations.

As a result of multiple correlation analyses of these data three experiments were conducted. Results of these experiments, which demonstrate that it is possible to modify the heat wave problem by application of various ground cover materials, are also presented.

NAVWEPS REPORT 7773

time intervals at various distances and from several camera elevations.

As a result of multiple correlation analyses of these data three experiments were conducted. Results of these experiments, which demonstrate that it is possible to modify the heat wave problem by application of various ground cover materials, are also presented.

CONTENTS

Figures:

INTRODUCTION

Until the most recent times man has humbly accepted limitations of visibility and the accompanying curtailment of his activities wherever and whenever such limitations occurred. Fog-horns, radar, and sonar are examples of modern devices and techniques used to either implement visibility or compensate for lack of visibility. During the past twenty-five years the acceleration of advances in technology particularly in applications to new ordnance and to space exploration have intensified man's interest and progress in visibility problems. Laboratories have been established which are devoted exclusively to problems in visibility.

Test objects are usually viewed or photographed over some path of sight through the atmosphere. The classic principles of optics tacitly assume a steady isotropic atmosphere in the interests of simplicity. The atmosphere, however, is subject to the convective disturbances of heat waves variously referred to as shimmer, heat boil, differential refraction, or, in the case of stars, twinkle. These disturbances are especially important in measurements made over the long reaches of terrain at the Nation's several missile test centers.

Heat waves, optical haze, and similar phenomena have been little studied with respect to their effects on the resolving power of an optical system or the displacements and distortions of the resulting photographic images. Most of the past work in this field has been devoted to measuring the limits of distant vision of certain objects, or the attenuation of contrast of distant objects having various patterns or surface markings. Except for the foundational work of Ward (Refs. 29 and 31) and some miscellaneous investigations published in one or two memoranda little actual work on this problem took place at NOTS prior to 1953. Yet in spite of scanty experimental data this troublesome problem was the subject of much discussion and occasional controversy.

In September 1953 the late William H. Christie began searching the literature and studying the feasibility of an experimental determination of the important factors producing this disturbance, and of the possible steps to be taken to alleviate, in part, the problems associated with heat waves. Christie was aided in this investigation by several other Station scientists, who carried on the work after his untimely death until such time as they were transferred to other projects, whereupon the project came to a standstill, unfinished and essentially unreported. The greater portion of this report deals with the work of Christie and his associates.

The report is divided into five parts: The first part deals with the establishment of the Heat-Wave range; the second with the test results from the range; the third, "Peregrinations of Optical Images", though partly theoretical, incorporates results from measurements made on Station; the fourth, "Ground-Cover Studies", reports work done largely by Carroll L. Evans, Jr. and Lynn L. Lyon to determine what effects various ground cover materials in the camera vicinity would have on photographic resolution; the fifth part sets forth conclusions. Appendix A is a description of test range instrumentation. Mathematical derivations and experimental details appear in Appendices B and C.

ESTABLISHMENT OF THE HEAT-WAVE RANGE

Preliminary investigation had indicated that many different factors might be responsible for heat waves, and that other phenomena such as haze, cloud cover, and wind velocity, contributed to resolution problems. It was at once apparent that controlled experiments were impractical as an incidental adjunct to normal use of the ordnance test ranges. It was thus necessary to set up a separate range for such studies, and in November 1954 a test array, to be known as the Heat-Wave Range, was established by Christie at K-2 range.

The purpose of the Heat-Wave Range was to study the effects of heat waves on visual and photographic images. The range consisted essentially of a Mitchell camera having a 48-inch lens, the camera being mounted on an elevator platform and used to photograph a series of resolution targets at distances up to 4,000 ft from camera heights varying up to 30 feet. Instrumentation of the range is described in detail in Appendix A. Examples of the variations of resolution with time of year and camera height are shown in Fig. 1.

4 Air Proving Ground Center, Eglin Air Force Base (Members, Optical Systems Working Group, IRIG)
5 Eglin Air Force Base
  Steering Committee Member, IRIG (1)
  Members, Optical Systems Working Group, IRIG (2)
  Member, Photographic Processing Working Group, IRIG (1)
  Member, Meteorological Working Group, IRIG (1)
1 Holloman Air Force Base (Member, Optical Systems Working Group, IRIG)
1 Rome Air Development Center, Griffiss Air Force Base
10 Armed Services Technical Information Agency (TIPCR)
1 Director of Defense (R&E) (Steering Committee Member, IRIG)
3 National Aeronautics & Space Administration
  Steering Committee Member, IRIG (1)
  Member, Meteorological Working Group, IRIG (1)
  Member, Optical Systems Working Group, IRIG (1)
2 National Bureau of Standards
  Office of Basic Instrumentation (1)
  Steering Committee Member, IRIG (1)
1 Applied Physics Laboratory, JHU, Silver Spring (Technical Document Center)
1 AVCO Research Laboratory, Everett, Mass. (Document Control Center)
1 California Institute of Technology, Pasadena (Library)
2 General Dynamics, Pomona, Calif. (Missile Division)
1 Harvard College Observatory, Cambridge
2 Jet Propulsion Laboratory, CIT, Pasadena
  R. A. Becker (1)
1 Lick Observatory, Mt. Hamilton, Calif.
1 Lincoln Laboratory, MIT, Lexington
1 Lowell Observatory, Flagstaff, Ariz.
2 Massachusetts Institute of Technology, Cambridge
  Research Laboratory of Electronics (1)
  Servomechanisms Laboratory (1)
1 Mt. Wilson Observatory, Pasadena
1 Northwestern University, Evanston, Ill.
1 Oregon State University, Corvallis (Library)
1 Portland State College, Portland, Oreg. (Library)
3 Sandia Corporation, Albuquerque
  Steering Committee Member, IRIG (1)
  Members, Optical Systems Working Group, IRIG (2)
1 Stanford University, Stanford, Calif. (Library)
1 The Rand Corporation, Santa Monica, Calif.
1 The University of Michigan, Ann Arbor
1 University of California, Berkeley
1 University of California, Los Angeles (Engineering Department, Dr. T. A. Rogers)
1 University of Denver, Denver Research Institute, Denver
1 University of New Mexico, Albuquerque (Physical Science Laboratory)
1 University of Southern California, Los Angeles (Library)
1 Yerkes Observatory, University of Chicago